Ore Geology Reviews 141 (2022) 104650

Contents lists available at ScienceDirect

Ore Geology Reviews

journal homepage: www.elsevier.com/locate/oregeorev

Geochemical, isotopic and U-Pb geochronological investigation of the late Cretaceous Karaçayır carbonatite (Sivas, Turkey): Insights into mantle sources within a post-collisional tectonic setting

Okay Çimen [a,*], Haşim Ağrılı [b], Corinne Kuebler [c], Antonio Simonetti [c], Loretta Corcoran [c], Stefanie Simonetti [c], Turgut Çolak [b], Sedat İnal [b], Cahit Dönmez [b]

[a] Munzur University, Rare Earth Elements Application and Research Center, 62000 Tunceli, Turkey
[b] General Directorate of Mineral Exploration and Research, 06530 Ankara, Turkey
[c] University of Notre Dame, Department of Civil and Environmental Engineering and Earth Sciences, South Bend, IN 46556, USA

ARTICLE INFO

Keywords:
Carbonatites
Isotopes
Mantle source heterogeneity
Open system behaviour
Recycled crustal carbon
Post-collisional tectonic setting

ABSTRACT

The Karaçayır carbonatite is located within the northeastern edge of the Central Anatolian Crystalline Complex, and represents one of the significant rare earth element (REE) mineralizations in Turkey. The carbonatite intrudes the associated syenite as dikes and veins, and is mainly composed of medium- to coarse-grained calcite, and lesser amounts of apatite, mica, amphibole, pyroxene, and magnetite. This study reports new and combined geochemical, radiogenic (Sr, Pb), stable (O and C), and for the first time B and Nd isotopic ratios and in-situ U-Pb age data from the Karaçayır carbonatite. The carbonate separates from the Karaçayır carbonatite are characterized by high Ba (30 to 484 ppm), Sr (613 to 9106 ppm) and total rare earth element (TREE) concentrations (172 to 2892 ppm), which are consistent with geochemical signatures for mantle-derived carbonate melts. The combined $\delta^{18}O_{V\text{-}SMOW}$ (+10.7 to +19.0 ‰), $\delta^{13}C_{V\text{-}PDB}$ (−2.9 to +1.8 ‰) and $\delta^{11}B$ (−13.9 to −2.9 ‰) data for a majority of the carbonate separates investigated here in contrast indicate that they are the result of open system behavior involving contamination by the country rock (marble), and/or sub-solidus, low temperature alteration. Based on the combined stable and radiogenic isotopic signatures for the least altered/contaminated samples, the carbonatite magma at Karaçayır most likely represents a low-degree partial melt of an isotopically heterogeneous (metasomatized) mantle source containing EM (enriched mantle)-like components and recycled crustal carbon; the latter finding is consistent with those recorded for young (<300 Ma old) carbonatites worldwide. A weighted mean $^{206}Pb/^{238}U$ age of 69.3 ± 1.7 Ma is obtained for apatite from the Karaçayır carbonatite, and indicates its emplacement within a post-collisional tectonic setting during the late Cretaceous.

1. Introduction

Rare earth elements (REEs) are critical components for high-tech industries including defense and space, e-mobility and renewables due to their unique physical and chemical properties (Goodenough et al., 2016; European Commission, 2020). Today, around 70% of the global supply of REEs is controlled by China (Statista, 2020; USGS, 2020), and may thus present an issue with provision for many international users; in particular those which have to import essentially all their REE requirements, either as raw materials or derivative products such as batteries and magnets (Machacek and Kalvig, 2016). In the next decade, it is estimated that the demand for REEs, such as Nd, Dy, La, Pr and Ce will dramatically rise due to the increasing high-tech activities and their usage in green energy infrastructures (e.g., Dushyantha et al., 2020). Therefore, it becomes imperative that consumer countries attempt to establish their own REE supply chains with reliable supplier countries in order to protect productive activities in their strategic economic sectors.

REE resources worldwide are predominantly associated with carbonatites (62%), alkaline complexes (16%), iron oxide copper gold deposits (IOCG, 15%), placers (5%), and ion-adsorption clay deposits (1%) (Zhou et al., 2017 and references therein). Therefore, carbonatite represents one of the most important rock types for REE exploration and related mining industry, and such complexes are found in continental rifts, orogenic belts, and even oceanic environments (e.g., Woolley,

* Corresponding author.
E-mail address: okaycimen@gmail.com (O. Çimen).

https://doi.org/10.1016/j.oregeorev.2021.104650
Received 3 August 2021; Received in revised form 9 December 2021; Accepted 13 December 2021
Available online 16 December 2021

1989; Mitchell, 2005; Kogarko et al., 2009; Kynicky et al., 2012; Chakhmouradian et al., 2012, 2015; Vrublevskii et al., 2019; Annenburg et al., 2020). Mining activities associated with carbonatites, alkaline complexes, and laterite deposits located in the east and southeast Asia (e.g., Bayan Obo, Weishan and Xunwu/Longnan) provide the predominant REE supply to international markets; other potential areas with economic concentrations of REEs are mainly concentrated in Australia (e.g., Nolans Bores), South Africa (e.g., Steenkampskraal), and North America (Bear Lodge; Walters et al., 2011; Barakos et al., 2015).

In addition to the significant economic interest related to REE deposits associated with carbonatites cited above (may also contain economic concentrations of Sr, P, Ta, and Nb), the origin of carbonatitic melt, which may represent the source for the REE mineralization, remains a matter of debate. Three main hypotheses have been proposed for the genesis of carbonatitic magma (summarized in Bell et al., 1998): a. It represents residual melt from a fractionated carbonated, parental nephelinite or melilitite magma, b. Formed as an immiscible melt fraction from CO_2-saturated, alkaline Si-undersaturated magma, and c. Generated as primary mantle melt via partial melting of CO_2-bearing peridotite (Jones et al., 2013 and references therein). Moreover, the origin of carbon (C) in carbonatite and its mantle source is also still poorly understood, as it may be either juvenile (primordial) or recycled, or a combination of both (Bell and Simonetti, 2010; Hulett et al., 2016). Recently, the use of boron (B) isotope signatures combined with other stable (O, C) and radiogenic (Sr, Nd, Pb) isotope compositions of carbonatites worldwide have provided significant and useful insights on the origin and petrogenetic evolution of C in the upper mantle (Hulett et al., 2016; Çimen et al., 2018, 2019, 2020; Kuebler et al., 2020, in press). Hence, additional geochemical and isotopic investigations of carbonatites, in particular those from relatively unexplored regions of the globe, or areas of varying tectonic environments may provide critical insights into the mantle carbon cycle and their mode of formation. Consequently, the chemical nature of their upper mantle source region and the tectonic/geodynamic evolution processes involved may be

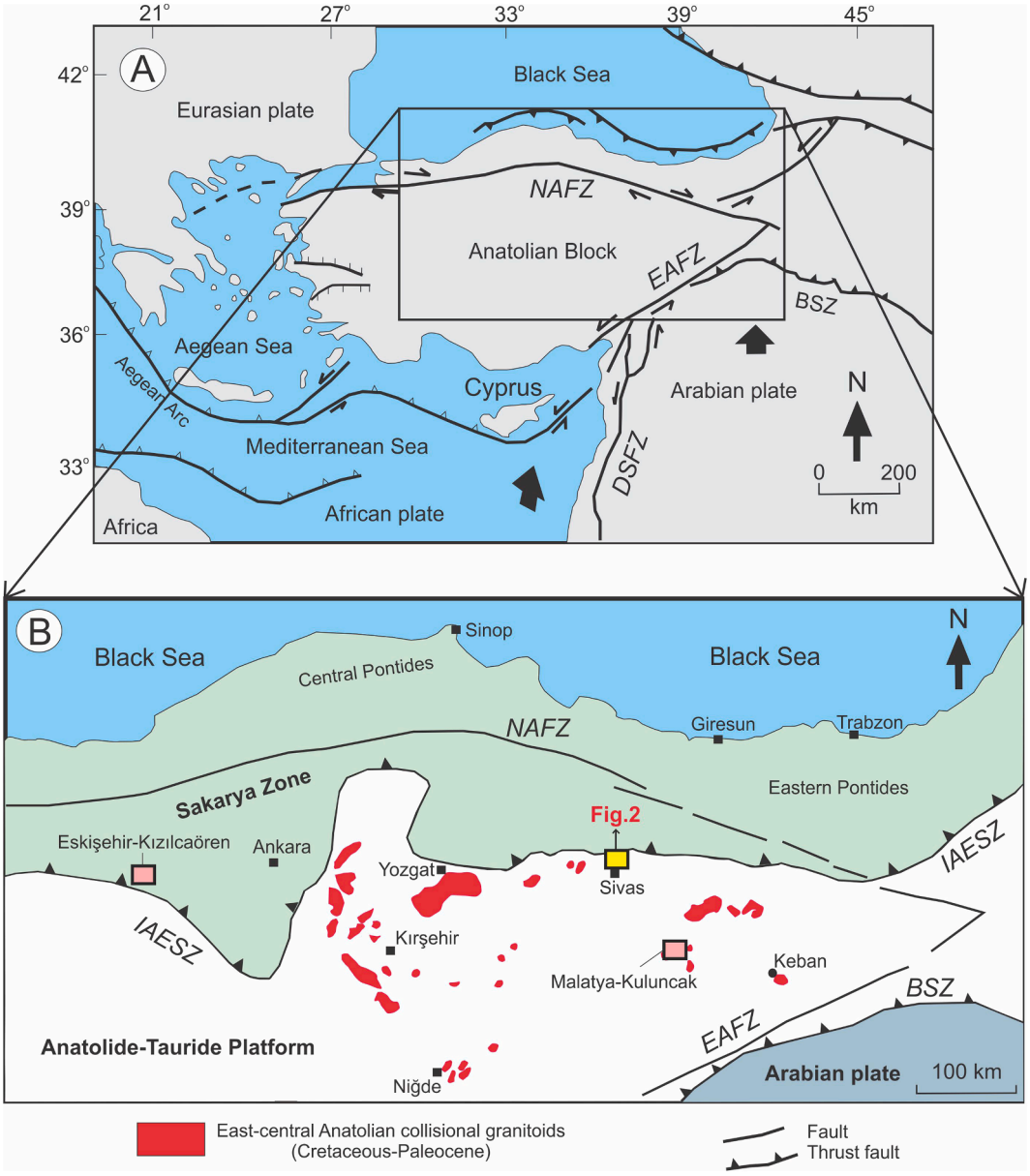

Fig. 1. A. Tectonic map of Turkey (modified from Boztuğ et al., 2007; Çimen et al., 2020), and **B.** Distribution of the Createcous-Paleocene collisional granitoids in east-central Turkey and the other REE deposits (Eskişehir-Kızılcaören and Malatya-Kuluncak; modified from Boztuğ et al., 2007; Çimen et al., 2020). NAFZ: North Anatolian Fault Zone, EAFZ: East Anatolian Fault Zone, DSFZ: Dead Sea Fault Zone, IAESZ: Izmir-Ankara-Erzincan Suture Zone, BSZ: Bitlis-Zagros Suture Zone.

better understood, which may in turn be used to explore both their possible lineage and occurrences for new REE deposits worldwide.

The main REE metallogenic provinces in Europe (Goodenough et al., 2016) include the Gardar Province (south-west Greenland), the Proto-gine Zone (southern Sweden), the Kola Alkaline Province (north-west Russia), the Oslo Rift (Norway), and the Anatolian Rift (western Turkey). The REE deposits associated with the Anatolian Rift within Turkey (Fig. 1 are the least known despite the presence of significant REE occurrences, such as the Eskişehir-Kızılcaören (~4.67 Mt with 2.78 wt% average grade; Öztürk et al., 2019a), the Malatya-Kuluncak, and the Sivas-Karaçayır; the tonnage and grade for the latter two deposits are still currently under evaluation. The Anatolian block represents the amalgamation of several small tectonic terranes or continental plates (e.g., İstanbul-Zonguldak, Sakarya and Anatolide Tauride) resulting from the closure of different branches of the Tethyan Ocean (Fig. 1; e.g., Şengör and Yılmaz, 1981; Göncüoğlu et al., 1997). These geodynamic processes have resulted in the formation of several magmatic complexes that host significant mineral deposits thoroughout the Anatolian Belt (e.g., Kuşçu et al., 2013 and references therein). One of these large-scale igneous provinces/associations, the Central Anatolian Crystalline Complex (CACC), covers an extensive area within central and east-central Turkey (Fig. 1, Göncüoğlu et al., 1991). The CACC includes a variety of magmatic intrusions (e.g. granite, monzonite, syenite) that range in chemical composition from calc-alkaline to alkaline (Lefebvre, 2011 and references therein).

The largest REE deposit in Turkey, the Eskişehir-Kızılcaören, is located in western Turkey, but other important REE deposits are present, such as the Malatya-Kuluncak and the Sivas-Karaçayır, and these are hosted by the central and east central Anatolian collisional granitoids (Fig. 1; Özgenç, 1993; Öztürk et al., 2019a,b; Çimen et al., 2020). With regards to the origin of the Eskişehir-Kızılcaören deposit, two formation models have been proposed: a. Hydrothermal mineralization associated with the alkaline volcanism (e.g., Kaplan, 1977; Gültekin et al., 2003), and b. Carbonatite-hosted REE mineralization (e.g., Daleloye and Özgenç, 1983; Özgenç, 1993, Nikiforov et al., 2014). On the other hand, carbonatite-hosted/associated type mineralization has been proposed for the genesis of the Malatya-Kuluncak deposit (e.g., Özgenç and Kibici, 1994; Özgenç and İlbeyli, 2009; Öztürk et al., 2019a,b). However, Çimen et al. (2020) reported for the first time combined radiogenic (Sr, Nd, Pb) and stable (C, O, B) isotopic data from these deposits, and suggested that the REE mineralization in the Eskişehir-Kızılcaören region may potentially be related to carbonatite magmatism, whereas the mineralization in the Malatya-Kuluncak region involved hydrothermal/magmatic fluids associated with extensive post-collisional magmatism. Recently, a crust-derived carbonatite occurrence has been reported from the eastern Armutlu Peninsula (NW Turkey), but it is characterized by low incompatible elements (e.g. Ba, Th, Nb) and total REE contents (11–91 ppm) compared to mantle-derived carbonatites (Özkan et al., 2021).

An additional, significant REE deposit from Turkey occurs within the Sivas-Karaçayır complex, which is located at the northeastern edge of the CACC and is associated with carbonatite magmatism (Fig. 1; Schuiling, 1961; Cooper et al., 2011). Schuiling (1961) first suggested that protruding segments of the country rock marble (a member of Akdağ metamorphic rocks; Fig. 2 into the syenite magma during emplacement were consequently transformed into a carbonatite-pegmatite. Subsequently, Cooper et al. (2011) reported chemical and stable/radiogenic isotope data from syenite, carbonatitic formations and marbles, and alternatively proposed that the carbonatite represents the product of fractional crystallization of syenite magma. In this study, we report new and combined geochemical data, radiogenic (Sr, Pb), stable (O and C), and for the first time Nd and B isotope compositions, and in-situ U-Pb age data for carbonatites from the Sivas-Karaçayır region. The main objectives are to better understand their petrogenetic evolution, tectonic setting during emplacement, and chemical nature of their mantle source(s). In addition, the results obtained in this study are compared to those from the other REE deposits (Eskişehir-Kızılcaören and Malatya-Kuluncak) in Turkey to decipher their mantle source regions within the geodynamic context and tectonic evolution of the Anatolian block.

2. Geological background

The CACC consists of various metamorphic massifs (Akdağ, Kırşehir, Niğde), plutons varying from granitic to syenitic composition and fragmented ophiolites, and these crystalline units are unconformably overlain by Tertiary volcanic and sedimentary units (Göncüoğlu et al., 1991; İlbeyli et al., 2009; Beyazpirinç et al., 2021). These metamorphic

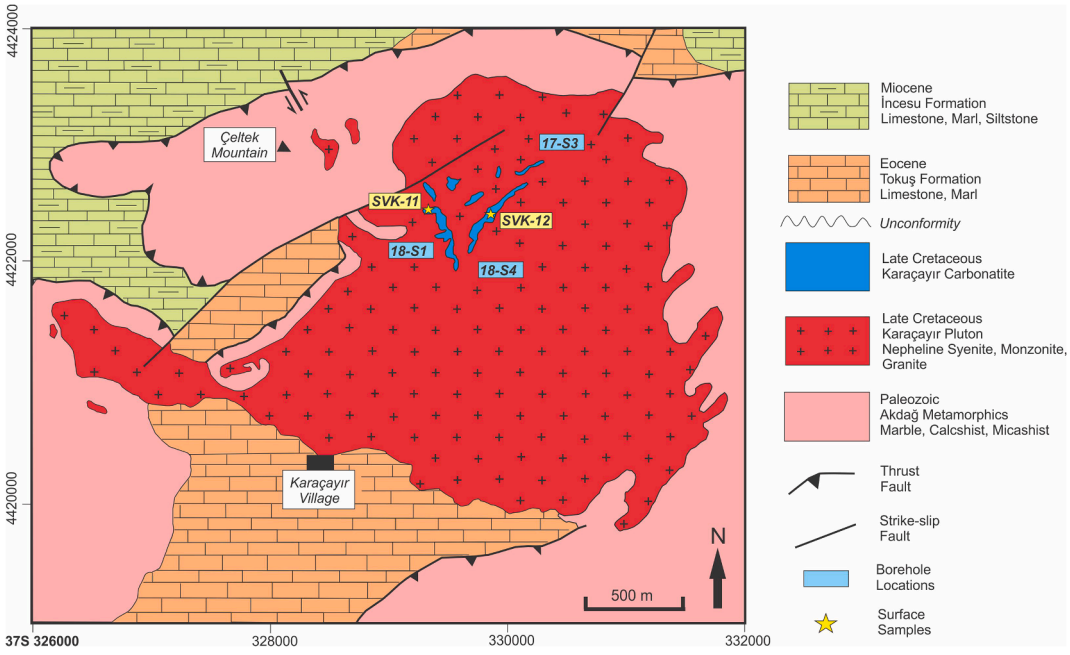

Fig. 2. Geological map of the Sivas- Karaçayır region including borehole locations (modified from MTA, 2002). See Table 1 for boreholes and sample depths.

massifs represent the cores of the complex, and consist of numerous rock types such as gneiss, schist, amphibolite and marble that formed under various temperature and pressure conditions (700–800 °C and 6–8 kbar) in the Late Cretaceous (91–84 Ma) period (Koçak and Leake, 1994; Whitney and Hamilton, 2004; İlbeyli et al., 2009). The ophiolitic units in the region are largely represented by the Late Cretaceous (90–85 Ma) intra-oceanic subduction products, which consists of basalt, radiolarian chert, pelagic limestone and sandstone in an Upper Cretaceous serpentinite matrix (Floyd et al., 2000; Yaliniz et al., 2000; Lefebvre, 2011). The magmatic rocks that intruded into the metamorphic and ophiolitic units are composed of granitic, granodioritic, monzonitic and syenitic intrusions that are calcalkaline and alkaline in composition displaying I, S and A type characteristics (Boztuğ, 1998; Lefebvre, 2011 and references therein). In trace element discrimination diagrams, these magmatic rocks plot within the island arc, intracontinental, collision or post-collision granitoid fields (e.g., Aydın et al., 1998; İlbeyli et al., 2004, Lefebvre, 2011). Ages ranging from 75 to 95 Ma have been reported for these intrusions by several previous studies (e.g., Güleç, 1994; Boztuğ, 1998; Whitney et al., 2003; Köksal et al., 2004; Boztuğ et al., 2007; Lefebvre, 2011) using various radiometric dating methods (e.g., whole rock Rb-Sr, biotite K-Ar, zircon and titanite U-Pb and zircon Pb-Pb evaporation). Moreover, İlbeyli (2005) and Boztuğ et al. (2007) have suggested that the crystallization of these intrusions took place at temperatures and pressures of approximately 600–750 °C and 2.5–4.5 kbar, respectively.

The Karaçayır Pluton is located in the northeastern part of the CACC and consists of an intrusive body that is 4 km by 3.5 km. Based on field relationships, this pluton intruded into the Akdağ Metamorphic units, and is unconformably overlain by the Paleocene-Eocene Tokuş formation (at the south-west boundary), which consists of units such as conglomerate, sandstone, limestone, marl and siltstone (Figs. 2, 3a; İnan and İnan, 1999, Boztuğ et al., 2009). All these units in the region are overlain by the Miocene-aged cover (İncesu formation), which mainly comprises limestone, marl and siltstone (Fig. 2. The Karaçayır Pluton is composed mainly of syenite and lesser amount of monzonite and granite (Fig. 3b, c, d; Boztuğ et al., 2009; Cooper et al., 2011). Moreover, the existence of carbonatitic rocks (Fig. 3e, f within the pluton was first documented by Schuiling (1961). Late Cretaceous crystallization (zircon evaporation U-Pb = 99.0 ± 11.0 Ma, Boztuğ et al., 2007; zircon U-Pb = 67.8 ± 1.1 Ma, Cooper et al., 2011) and the Paleocene cooling ages (biotite Ar-Ar = 65–66 Ma; Boztuğ et al., 2009) have been reported for syenitic rocks within the Karaçayır Pluton.

Based on field observations, the carbonatite intrudes into the syenite as dykes and veins (from ~ 10–15 cm to ~ 3–4 m thicknesses; Figs. 2, 3b, and these generally consist of medium- and coarse-grained calcite with lesser amounts of apatite, mica, amphibole and magnetite. Here, coarse-grained mica and apatite crystals are observed in several handspecimens (Fig. 3e, f. It should be noted that no marble inclusions in syenite were intersected by the boreholes investigated here (Table 1, Fig. 3f. Grains of mica, apatite, amphibole and magnetite are hosted predominantly within a coarse-grained calcite groundmass (Fig. 4. The mica crystals show brownish colors with subhedral to euhedral shapes, and represent

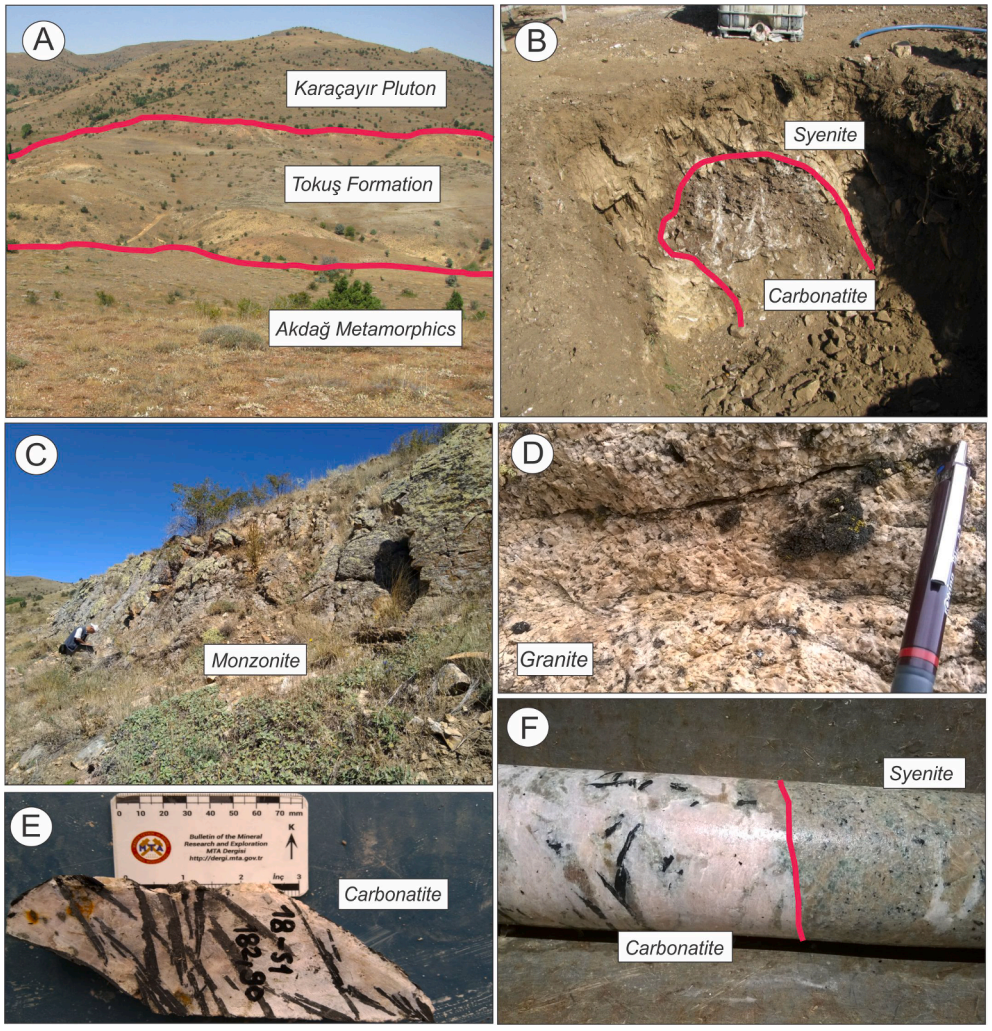

Fig. 3. A. Main geological formations in the study area (the cross-cutting contact between the Karaçayır Pluton and the Akdağ Metamorphics is unconformably overlain by the Tokuş Formation). **B.** An image illustrating the cross-cutting relationship between the carbonatite and altered syenite in the Karaçayır Pluton. **C.** Field image of the monzonite from the Karaçayır Pluton. **D.** Field image of the granite from the Karaçayır Pluton. **E.** An image showing coarse mica crystals from the Karaçayır carbonatite (white parts are mostly composed of calcite and apatite grains). **F.** An image from drilling core that illustrates the cross-cutting relationship between the carbonatite and syenite.

Table 1
Trace element concentrations for calcite separates from the Karaçayır carbonatites.

Sample	SVK-1	SVK-2	SVK-4	SVK-5	SVK-6	SVK-7	SVK-8	SVK-9	SVK-10	SVK-11	SVK-12
Borehole Name	18-S1	18-S1	18-S4	18-S4	18-S4	18-S4	17-S3	17-S3	17-S3	surface	surface
Depth	183 m	184 m	218 m	224 m	319 m	314 m	101 m	33 m	168 m		
B	2.64	2.98	0.76	3.84	0.58	1.51	2.37	0.93	4.72	1.30	1.46
Cs	0.03	0.03	*b.d.*	0.01	0.01	*b.d.*	0.04	0.11	0.02	*b.d.*	0.01
Rb	0.45	0.87	0.08	0.02	0.20	0.03	0.07	2.61	0.11	0.14	0.10
Ba	382	73.8	483	53.9	48.6	142	213	53.8	29.9	63.3	302
Th	2.11	7.82	1.14	1.23	4.26	1.96	1.40	1.68	1.43	0.96	5.42
U	2.36	1.80	0.21	0.05	1.61	0.06	0.96	0.93	0.33	0.17	0.82
Nb	0.47	0.71	0.04	0.08	0.14	0.04	0.32	0.46	0.10	0.18	0.20
La	327	491	130	83.4	56.1	412	724	179	89.5	394	685
Ce	669	808	154	105	80.9	372	1331	313.	203	705	1307
Pb	24.2	12.0	43.0	35.2	15.9	25.3	36.0	19.6	32.5	30.6	38.0
Pr	64.5	83.8	12.9	8.70	6.60	30.5	119	25.7	16.3	69.8	123
Mo	0.14	0.25	0.07	1.45	0.13	0.20	0.25	0.14	0.29	0.25	0.18
Sr	4185	2081	1176	878	613	2536	9106	1126	816	6319	8329
Nd	268	367	39.8	27.3	19.8	99.6	509	80.0	52.0	302	450
Sm	46.4	61.7	4.70	3.50	2.60	12.6	72.0	10.0	6.60	49.5	65.1
Zr	0.14	0.21	0.09	0.08	0.29	0.18	0.18	0.13	0.05	0.20	0.24
Eu	11.3	14.2	0.90	0.70	0.60	2.60	15.6	2.10	1.40	11.7	14.4
Gd	34.5	44.4	2.70	2.50	2.10	7.20	47.5	5.80	4.40	34.5	43.0
Tb	4.32	5.34	0.34	0.33	0.27	0.87	5.61	0.71	0.56	4.29	5.46
Dy	23.2	28.5	1.60	1.80	1.40	4.50	28.7	3.80	3.00	23.3	27.5
Li	0.17	0.37	0.04	0.02	0.10	0.01	0.02	0.43	0.08	0.15	0.04
Y	96.1	175	16.8	16.2	11.5	45.7	139	21.5	17.6	106	147
Ho	4.32	5.19	0.32	0.34	0.29	0.83	5.26	0.71	0.63	4.21	5.09
Er	12.2	14.4	0.92	0.99	0.81	2.26	14.8	1.97	1.74	12.2	14.4
Tm	1.57	1.93	0.12	0.12	0.11	0.32	1.92	0.26	0.24	1.73	1.99
Yb	11.2	13.2	0.89	0.83	0.69	2.08	13.2	1.75	1.68	11.5	13.4
Lu	1.66	1.91	0.12	0.11	0.10	0.28	1.91	0.27	0.21	1.66	1.97
$La/Lu_{(CN)}$	21	28	117	81	61	161	41	73	45	26	37

Note: b.d. = below detection limit.

the second most common phase in the carbonatites. The apatite crystals exhibit greyish interference colors, and overall have subhedral to euhedral shapes. The amphiboles show greenish color and exhibit subhedral to anhedral shapes. Lastly, magnetite represents the dominant opaque mineral phase in the carbonatite and displays euhedral shapes (Fig. 4c. In addition to the mineral paragenesis given here, K-feldspar, albite, thorianite, monazite and allanite have also been identified within the carbonatite (Schuiling, 1961; Cooper et al., 2011).

3. Analytical methods

A total of 9 representative samples of the Karaçayır carbonatite were taken from three boreholes, whereas 2 samples (SVK-11 and −12) were collected from surface outcrops (Fig. 2. The borehole and sample numbers and their corresponding depths are given in Table 1. Detailed chemical and isotopic analyses were conducted on calcite separates that were hand-picked under a binocular microscope. The semi-quantitative chemical maps shown in Fig. 4 were obtained using an Edax Orbis μ-XRF instrument at the Center for Environmental Science and Technology (CEST), University of Notre Dame. The operational conditions for this instrument: amplifier time of 12.8 μs, fluorescent energy of 32 kV, and beam size of 30 μm. Trace element concentrations were obtained via solution- (wet plasma) mode analysis using a Nu Plasma AttoM (high resolution) HR-ICP-MS instrument housed at the Midwest Isotope and Trace Element Research Center (MITERAC), University of Notre Dame. The $\delta^{18}O_{V\text{-}SMOW}$ and $\delta^{13}C_{V\text{-}PDB}$ isotope data for carbonate separates reported in this study (Table 2 were obtained using a Delta V Advantage isotope ratio mass spectrometer at CEST (University of Notre Dame). In addition, B, Sr, Nd and Pb isotope ratio measurements (Tables 2, 3 and 4 were determined via solution-mode on a Nu PlasmaII multi-collector (MC)-ICP-MS housed within MITERAC. Detailed analytical procedures for trace element abundance determinations and stable and radiogenic isotope analyses are described in Çimen et al. (2018, 2019) and Kuebler et al. (2020). Lastly, in-situ U–Pb age determinations for apatite crystals were also conducted by laser ablation- (LA)-MC-ICP-MS at MITERAC, and the analytical protocol and operational conditions are similar to those described in Chen and Simonetti (2014).

4. Results

4.1. Trace element abundances

Trace element concentrations obtained here for carbonate separates from the Karaçayır carbonatites are reported in Table 1. Fig. 5 displays the primitive mantle- (PM) and chondrite -normalized (CN) multi-element and REE patterns for the samples investigated here, respectively; these exhibit enrichments in Ba, Th, Sr and REEs that are consistent with those for carbonatites worldwide (e.g., Bell and Simonetti, 2010; Jones et al., 2013; Çimen et al., 2018, 2019) and the Eskişehir-Kızılcaören carbonatite (Çimen et al., 2020). The CN total REE (TREE) values for the samples studied here are between 44 and 708, whereas the PM-normalized values for Ba, Th and Sr range between 4 and 69, 11–92 and 39–432, respectively (Fig. 5. Also, the TREE concentrations for carbonate separates reported here vary between 236 and 2892 ppm (except for sample SVK-6 = 172 ppm; Table 1, and these abundances are mainly higher than those for whole rock sedimentary carbonates (<200 ppm, Xu et al., 2010). In addition, Ba (30 to 484 ppm), Th (0.96 to 7.82) and Sr (613 to 9106 ppm) contents of the samples studied here are also significantly higher than those for sedimentary limestone (Fig. 5a, Table 1. Moreover, in Fig. 5b, the enrichment in light-REEs over heavy-REEs ($La/Lu_{(CN)}$ = 21–161; Table 1 are indicative of typical magmatic carbonate, and these patterns are consistent with those previously reported by Cooper et al. (2011). Of note, the CN REE patterns for the samples investigated here define two distinct groups (Fig. 5b, and in particular those exhibiting the most enriched signatures overlap those reported for carbonatites and calcite syenites from Cooper et al. (2011).

In addition, the comparison of Sr, Ba and TREE contents of calcites

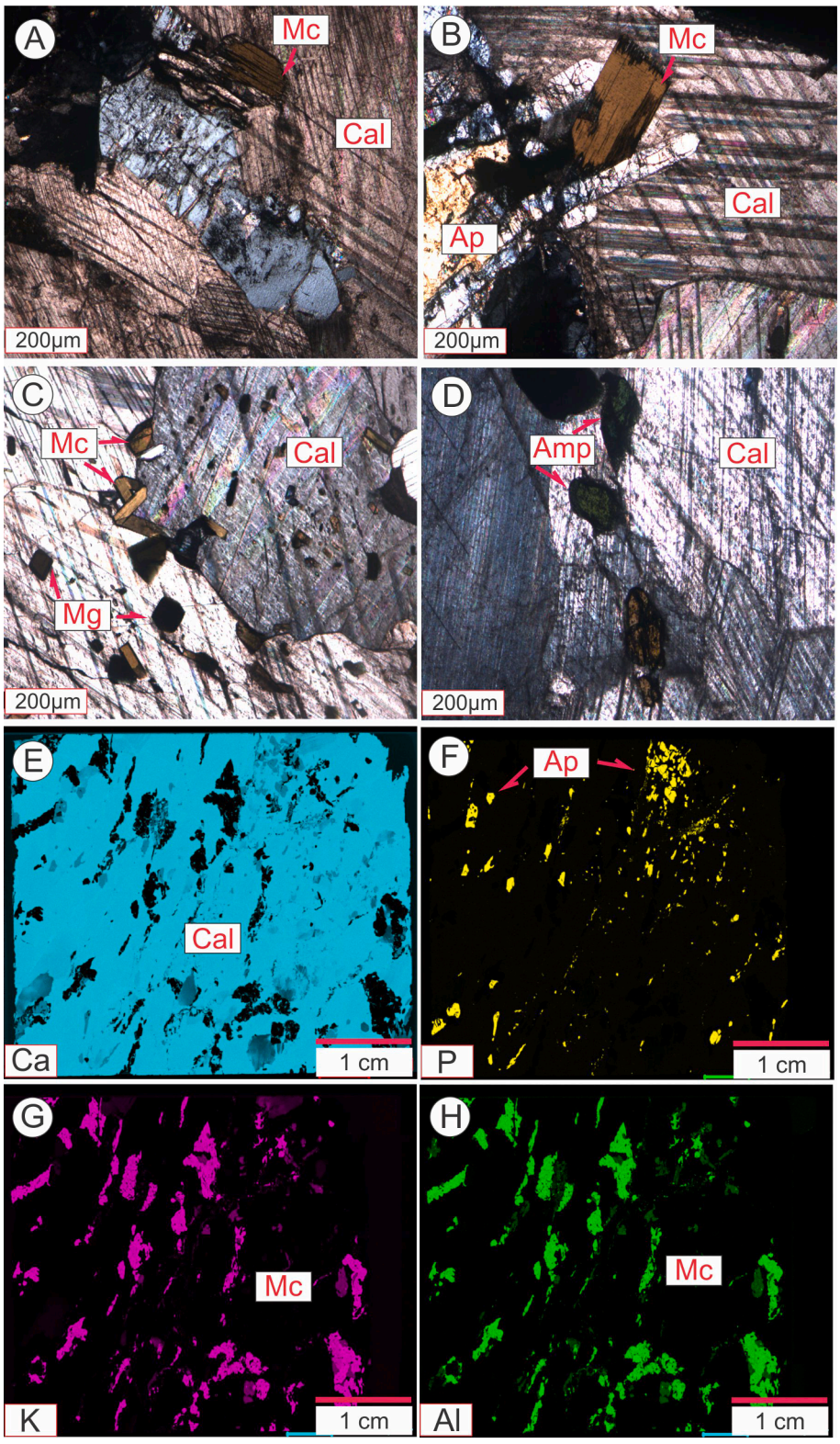

Fig. 4. A-D. Thin section and **E-H.** micro-XRF images from the carbonatite samples illustrating the presence of calcite (Cal), apatite (Ap), mica (Mc), amphibole (Amp) and magnetite (Mg) crystals.

from syenite, calcite syenite (Cooper et al., 2011) and carbonatite samples reported here (Table 1 display scattered distributions instead of any significant correlations, and the calcite crystals from most of the calcite syenite samples exhibit higher Sr and TREE contents compared to those from majority of carbonatites (Fig. 6. It has been recently well established that B contents are predominantly $\leq$ ~1 ppm for upper mantle-derived carbonatites (Hulett et al., 2016; Çimen et al., 2018, 2019, 2020; Kuebler et al., 2020), which overlap those for asthenosphere-derived, fresh (non-altered), mid-ocean ridge basalts (e.g., <1 ppm; MORBs; Spivack and Edmond, 1987; Wunder et al. 2005; Marschall et al., 2017). The first-reported B contents for the Karaçayır carbonatites (Table 1 vary between 0.6 and 4.7 ppm, and a majority of

Table 2
C, O, and B isotope data for calcite separates from the Karaçayır carbonatites.

Sample	$\delta^{13}C$ (‰)	σ	$\delta^{18}O$ (‰)	σ	$\delta^{11}B$ (‰) *
SVK-1	−2.86	0.05	11.44	0.09	−6.38
SVK-2	−2.93	0.03	10.99	0.08	−7.38
SVK-4	1.70	0.04	19.05	0.05	−25.9
SVK-5	1.81	0.03	14.47	0.07	−3.81
SVK-6	0.73	0.02	12.49	0.10	−3.01
SVK-7	0.99	0.01	13.13	0.07	−2.85
SVK-8	−2.93	0.03	10.69	0.10	−4.17
SVK-9	1.49	0.05	18.07	0.10	−6.88
SVK-10	1.72	0.04	14.50	0.07	−7.30
SVK-11	−2.47	0.04	10.72	0.09	−7.07
SVK-12	−2.60	0.04	10.79	0.09	−13.89

*Uncertainty associated with B isotope ratios is ± 0.5‰ (2 s level) based on replicate.
analyses of coral in-house standard.

them (except for samples SVK-5 and −9) are consistent with those for carbonatites worldwide and asthenospheric mantle. In addition, the B contents for the carbonatites investigated here are significantly lower than those for bulk continental crust (average = 10 ppm; Marschall et al., 2017), and the range documented for carbonate sediments (13–26 ppm; Ishikawa and Nakamura, 1993) and carbonates of biogenic origin (e.g., Kuebler et al., in press).

4.2. Stable isotope characteristics

Oxygen, carbon, and boron stable isotope data for calcite separates from the Karaçayır carbonatites are listed in Table 2 and illustrated in Figs. 7 and 8. The $\delta^{18}O_{SMOW}$ (‰) values for calcite separates investigated here range between +10.7 ‰ to +19.0 ‰, whereas the $\delta^{13}C_{PDB}$ (‰) values for the same samples vary between −2.9 ‰ to +1.8 ‰. The combined C and O isotope compositions plot outside and to the right of the field defined for "primary igneous carbonatites (PIC)" (Keller and Hoefs, 1995; Fig. 7. Five samples (SVK-1, −2, −8, −11, −12) are characterized by lighter O and C isotope values and plot proximal to the PIC box (Fig. 7, and represent the group of samples exhibiting the highest degree of REE enrichment (Fig. 5b; moreover, the C and O isotope compositions for this group of samples are similar to those for carbonates reported in Cooper et al. (2011). The remaining samples are characterized by significantly higher $\delta^{13}C_{PDB}$ and $\delta\ ^{18}O_{SMOW}$ values (Fig. 7 and contain significantly lower REE abundances (Fig. 5. It should be noted that the samples reported here have lighter O isotope values compared to those from the Eskişehir-Kızılcaören and the Malatya-

Table 3
Sr and Nd isotope data for calcite separates from the Karaçayır carbonatites.

Sample	Rb (ppm)	Sr (ppm)	$^{87}Rb/^{86}Sr$	$^{87}Sr/^{86}Sr$	2σ	$^{87}Sr/^{86}Sr$ *(i)*	Sm (ppm)	Nd (ppm)	$^{147}Sm/^{144}Nd$	$^{143}Nd/^{144}Nd$	2σ	$^{143}Nd/^{144}Nd$ *(i)*	εNd *(t)*
SVK-1	0.45	4185	0.00031	0.70768	0.00001	0.70768	46.4	268	0.1040	0.51235	0.00001	0.51230	−4.7
SVK-2	0.87	2081	0.00120	0.70773	0.00001	0.70773	61.7	367	0.1010	0.51234	0.00001	0.51229	−4.9
SVK-4	0.08	1176	0.00020	0.70708	0.00001	0.70708	4.70	39.8	0.0712	0.51238	0.00001	0.51234	−3.9
SVK-5	0.02	878	0.00008	0.70732	0.00001	0.70732	3.50	27.3	0.0776	0.51236	0.00001	0.51232	−4.3
SVK-6	0.20	613	0.00092	0.70752	0.00001	0.70751	2.60	19.8	0.0801	0.51238	0.00001	0.51234	−4.0
SVK-7	0.03	2536	0.00004	0.70702	0.00001	0.70702	12.6	99.6	0.0760	0.51235	0.00001	0.51231	−4.5
SVK-8	0.07	9106	0.00002	0.70772	0.00001	0.70772	72.0	509	0.0850	0.51234	0.00001	0.51230	−4.8
SVK-9	2.61	1126	0.00669	0.70707	0.00001	0.70706	10.0	80.0	0.0756	0.51236	0.00001	0.51233	−4.2
SVK-10	0.11	816	0.00038	0.70732	0.00001	0.70732	6.60	52.0	0.0761	0.51232	0.00001	0.51229	−5.0
SVK-11	0.14	6319	0.00006	0.70704	0.00001	0.70704	49.5	302	0.0984	0.51239	0.00001	0.51234	−4.0
SVK-12	0.10	8329	0.00004	0.70735	0.00001	0.70735	65.1	450	0.0869	0.51236	0.00001	0.51231	−4.4

Sr and Nd initial ratios and epsilon Nd values were calculated based on the 67 Ma age reported in this study. $^{87}Rb/^{86}Sr$ and $^{147}Sm/^{144}Nd$ values were calculated based on ICP-MS determined.
elemental abundances and are associated with relative uncertainties of between 3 and 5% (2σ level).

Table 4
Pb isotope data for calcite separates from the Karaçayır carbonatites.

Sample	U (ppm)	Pb (ppm)	Th (ppm)	$^{238}U/^{204}Pb$	$^{235}U/^{204}Pb$	$^{232}Th/^{204}Pb$	$^{206}Pb/^{204}Pb$	2σ	$^{207}Pb/^{204}Pb$	2σ	$^{208}Pb/^{204}Pb$	2σ
SVK-1	2.36	24.22	2.11	6.22	0.044	5.73	19.005	0.0004	15.731	0.0003	39.142	0.0010
SVK-2	1.80	12.03	7.82	9.57	0.068	42.84	18.997	0.0003	15.734	0.0002	39.186	0.0008
SVK-4	0.21	42.99	1.14	0.31	0.002	1.73	18.629	0.0003	15.694	0.0003	38.764	0.0010
SVK-5	0.05	35.17	1.23	0.10	0.001	2.69	30.058	0.0006	16.534	0.0004	39.550	0.0011
SVK-6	1.61	15.95	4.26	6.45	0.046	17.59	18.967	0.0003	15.726	0.0003	39.112	0.0008
SVK-7	0.06	25.26	1.96	0.15	0.001	5.10	18.953	0.0003	15.726	0.0003	39.121	0.0008
SVK-8	0.96	36.02	1.40	1.69	0.012	2.56	18.991	0.0002	15.734	0.0003	39.153	0.0008
SVK-9	0.93	19.60	1.68	3.04	0.022	5.66	18.978	0.0003	15.727	0.0003	39.129	0.0008
SVK-10	0.33	32.47	1.43	0.64	0.005	2.89	18.789	0.0002	15.714	0.0003	38.955	0.0009
SVK-11	0.17	30.59	0.96	0.35	0.003	2.07	18.980	0.0003	15.732	0.0003	39.145	0.0010
SVK-12	0.82	38.02	5.42	1.38	0.010	9.40	18.984	0.0003	15.730	0.0003	39.157	0.0010

Sample	$^{207}Pb/^{206}Pb$	2σ	$^{208}Pb/^{206}Pb$	2σ	$^{206}Pb/^{204}Pb$ *(i)*	$^{207}Pb/^{204}Pb$ *(i)*	$^{208}Pb/^{204}Pb$ *(i)*	$^{207}Pb/^{206}Pb$ *(i)*	$^{208}Pb/^{206}Pb$ *(i)*
SVK-1	0.82775	0.000005	2.060	0.00002	18.93	15.73	39.12	0.8307	2.066
SVK-2	0.82823	0.000004	2.063	0.00002	18.89	15.73	39.03	0.8328	2.066
SVK-4	0.84244	0.000005	2.081	0.00002	18.63	15.69	38.76	0.8426	2.081
SVK-5	0.55005	0.000004	1.316	0.00001	30.06	16.53	39.54	0.5501	1.315
SVK-6	0.82912	0.000005	2.062	0.00002	18.89	15.72	39.05	0.8322	2.067
SVK-7	0.82976	0.000005	2.064	0.00002	18.95	15.73	39.10	0.8298	2.063
SVK-8	0.82850	0.000006	2.062	0.00002	18.97	15.73	39.14	0.8293	2.063
SVK-9	0.82866	0.000004	2.062	0.00002	18.94	15.73	39.11	0.8301	2.064
SVK-10	0.83634	0.000006	2.073	0.00002	18.78	15.71	38.94	0.8366	2.074
SVK-11	0.82886	0.000006	2.062	0.00003	18.98	15.73	39.14	0.8290	2.062
SVK-12	0.82855	0.000007	2.063	0.00002	18.97	15.73	39.12	0.8292	2.063

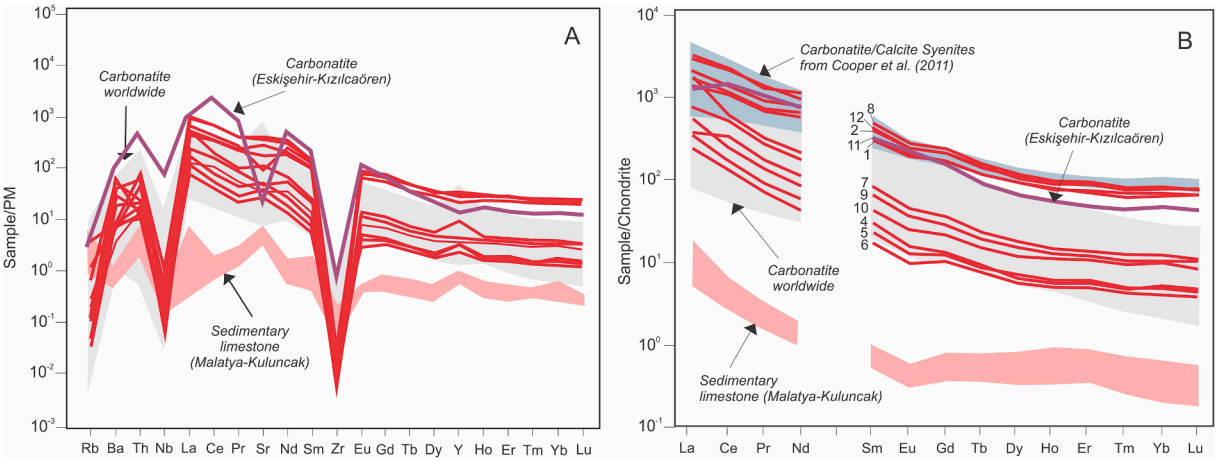

Fig. 5. A. Primitive mantle-normalized multi element patterns and **B.** Chondrite-normalized rare earth element patterns for carbonate separates from the carbonatite samples. Primitive mantle and chondrite values are from (Sun and McDonough 1989). Light gray field represents data for calcite separates from carbonatite worldwide (Çimen et al., 2018, 2019, 2020), whereas pink and light blue fields represent sedimentary limestone in the Malatya-Kuluncak Complex (Çimen et al., 2020) and carbonatites/calcite syenites in the Karaçayır Complex from Cooper et al. (2011), respectively. The purple line represents a carbonatite sample from the Eskişehir-Kızılcaören Complex (Çimen et al., 2020).

Kuluncak complexes. Also, the samples that plot close to the PIC field display lighter C isotope compositions than those from the Eskişehir-Kızılcaören and the Malatya-Kuluncak complexes.

The first-reported $\delta^{11}B$ (‰) values for carbonate separates from the Karaçayır carbonatite samples range between −3.0 and −25.9 ‰. With the exception of two samples (SVK-4 and −12; Table 2; Fig. 8, most of the samples (SVK-1, −2, −9, −10, −11) overlap (given their respective associated uncertainties) with the B isotopic value for asthenospheric mantle (~-7.1 ± 0.9 ‰; Marschall et al., 2017; Fig. 8. Here, the extremely lighter B isotope values of SVK-4 and −12 samples could have been resulted by low T alteration processes. Although four samples (SVK-5, −6, −7, −8) have slightly heavier B isotope values (−4.17 to −2.85‰; Table 2; Fig. 8 compared to asthospheric mantle, these are still consistent with those for mantle-derived (younger, <300 million years old) carbonatites worldwide (<+5.5‰; Hulett et al., 2016). The B isotope value for a carbonatite sample from the Eskişehir-Kızılcaören complex is consistent with those for the Karaçayır carbonatite samples and asthenospheric mantle (Fig. 8. In contrast, the sedimentary limestone samples from the Malatya-Kuluncak complex are characterized by heavier B isotope signatures, and plot close to the marine carbonate field (Fig. 8.

4.3. Radiogenic isotope signatures

The Sr, Nd, and Pb isotope data for carbonate separates from the Karaçayır carbonatites are listed in Tables 3 and 4, and illustrated in Figs. 9–12. In relation to the age corrections of the measured Sr, Nd, and Pb isotope ratios, an emplacement age of 69 Ma is used based on the in-situ U-Pb dating results for apatite within the carbonatites investigated here (described below). Since the $^{87}Rb/^{86}Sr$ values reported here (~0.0 to ~ 0.007) are low, the magnitude of the age correction of the measured $^{87}Sr/^{86}Sr$ ratios is insignificant for carbonate separates, and the calculated $^{87}Sr/^{86}Sr_{(i)}$ isotope values range between 0.70702 and 0.70773 (Table 3; Figs. 9, 10, 11. The $^{87}Sr/^{86}Sr_{(i)}$ values (Table 3; Fig. 11 reported here are similar to those (0.70732–0.70786) from Cooper et al. (2011). The $^{147}Sm/^{144}Nd$ ratios (~0.071 to ~ 0.104; Table 3 for the calcite separates examined here yield first-reported initial $^{143}Nd/^{144}Nd_{(i)}$ ratios that vary between 0.51229 and 0.51234 (Table 3, and these correspond to $\varepsilon_{Nd\ (69Ma)}$ values of −3.9 to −5.0 (Figs. 9, 10. The Sr and Nd isotope compositions for the Karaçayır carbonatite samples fall between the EM (enriched mantle) I and EMII fields (Zindler and Hart, 1986; Fig. 10a. Of note, carbonatite from the Eskişehir-Kızılcaören complex is characterized by a less radiogenic Sr isotope composition, whereas the Malatya-Kuluncak complex exhibits slightly more radiogenic Sr isotope signatures than those from the Karaçayır carbonatite samples investigated here (Fig. 10a; 11b). In addition, while the Eskişehir-Kızılcaören complex is characterized by more radiogenic Nd isotopes, the Malatya-Kuluncak complex shows a wider range compared to those for the Karaçayır carbonatite samples (Fig. 10a. Also, the marbles (country rock, Cooper et al., 2011) within the Karaçayır region are characterized by more radiogenic Sr isotope values than those from the carbonatite samples reported here (Fig. 11b. Lastly, initial Pb isotope compositions (Table 4; Figs. 11, 12 for carbonate separates from the Karaçayır carbonatites yield restricted ranges for $^{206}Pb/^{204}Pb_{(i)}$, (18.63 to 18.98), $^{207}Pb/^{204}Pb_{(i)}$ (15.69 to 15.73), $^{208}Pb/^{204}Pb_{(i)}$ (38.76 to 39.14), and the data for samples SVK-1, −2, −8, and −11 are consistent with those previously obtained by Cooper et al. (2011). Moreover, sample of SVK-5 is characterized by extremely high Pb isotope compositions compared to the remaining samples (Table 4; similar, elevated Pb isotope values have been previously reported from carbonatite occurrences worldwide (e.g., Andersen, 1987; Chen et al., 2018; Çimen et al., 2018, 2019). The initial Pb isotope compositions for carbonatite samples reported here plot close to the EMII field (Fig. 12. The Eskişehir-Kızılcaören and Malatya-Kuluncak complexes are characterized by slightly more radiogenic Pb isotope compositions compared to those from the Karaçayır carbonatite samples (Fig. 12. The marble xenoliths within the Karaçayır complex (Cooper et al., 2011) record less radiogenic Pb isotope signatures than those for most of the carbonatite samples investigated here (Fig. 12.

4.4. In-situ apatite U-Pb dating

In order to constrain the timing of carbonatite magmatism in the region, for the first time, the U-Pb isotope signatures of apatite from the Karaçayır carbonatites are reported here. The U–Pb geochronological data for apatite are listed in Table 5 and illustrated in Fig. 13. The in-situ U-Pb dating results for apatite from samples of SVK-1, −2, −8, and −12 (characterized by lightest C and O isotope compositions; Fig. 7 yield a concordia lower intercept age of 67.1 ± 2.4 Ma in a Tera-Wasserburg plot (Fig. 13a, corresponding to a weighted mean $^{206}Pb/^{238}U$ age of 69.3 ± 1.7 Ma (Fig. 13b. A range of crystallization ages (99.0 ± 11.0 Ma and 67.8 ± 1.1 Ma) have been previously reported for the syenites from the Karaçayır pluton (Boztuğ et al., 2007; Cooper et al., 2011).

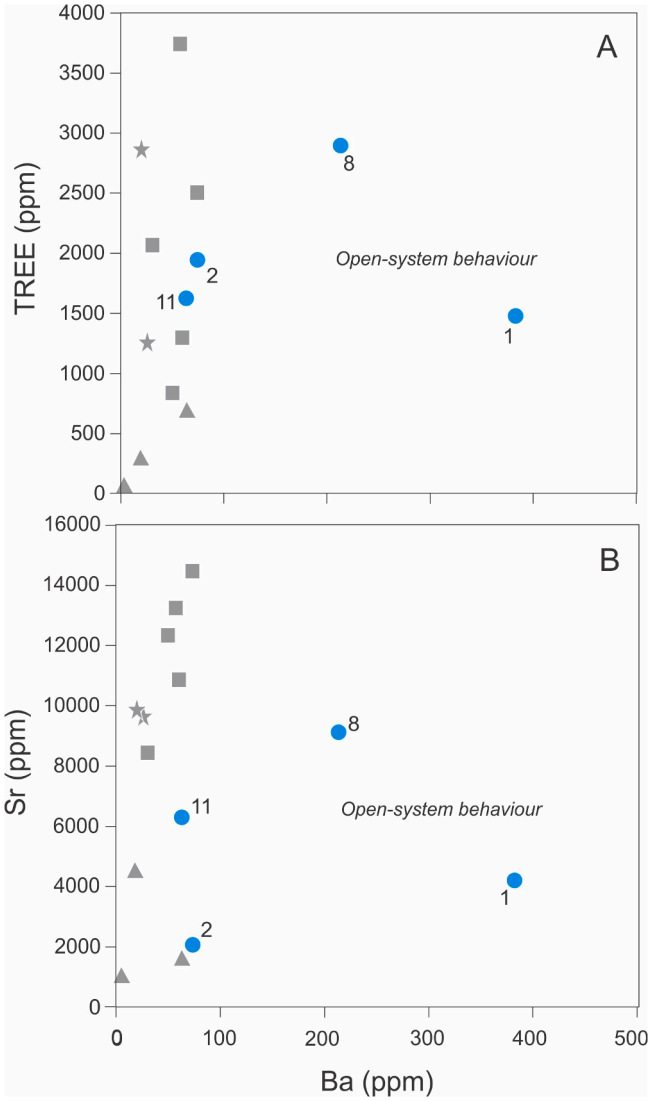

Fig. 6. Plots of **A.** total REE abundances (ppm) and **B.** Sr (ppm) vs. Ba (ppm) contents for calcites from syenite, calcite syenite and carbonatite samples from the Karaçayır Pluton. Gray triangle, square and star represent calcite crystals from syenite, calcite syenite and carbonatite samples, respectively and these data taken from Cooper et al. (2011). The blue circles represent the least contaminated/altered carbonatite samples investigated here.

5. Discussion

5.1. Role of crustal contamination/low temperature alteration

Mantle-derived carbonates can be distinguished from their sedimentary counterparts based on their field relationships (i.e., intrusion or lava flow), petrography and mineralogy, and just as importantly their geochemical and isotopic characteristics. Magmatic carbonates are mostly found associated with silica-undersaturated alkaline rocks (e.g., nepheline syenites, ijolites, phonolites) and ultramafic rocks (e.g., Bell et al., 1998; Mitchell, 2005; Woolley and Kjarsgaard, 2008), in the form of dikes, stocks, sills, veins or lavas (e.g., Rosatelli et al., 2000; Woolley and Church, 2005). In the Karaçayır pluton, the carbonatite bodies occur as dikes and veins that intrude the nepheline syenite (Fig. 3. In addition, they exhibit magmatic textures, which include the presence of apatite, mica, amphibole and magnetite hosted within a medium- and coarse-grained calcite matrix (Figs. 3, 4. Hence, these field relationships and petrographic features are characteristic of carbonate with magmatic lineage.

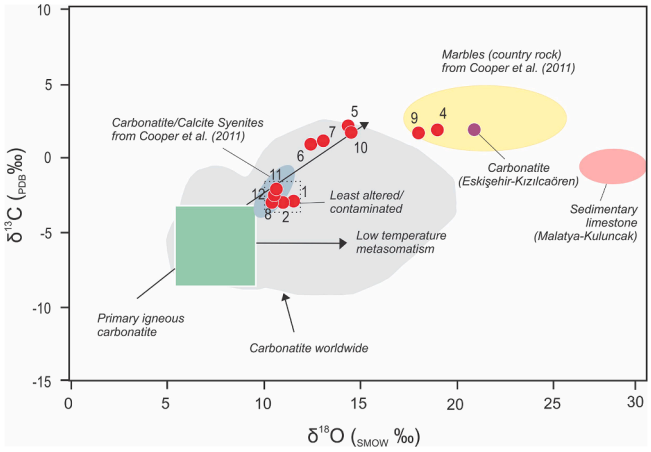

Fig. 7. Carbon and oxygen isotopic compositions for carbonate separates from the Karaçayır carbonatite samples. Primary igneous carbonatites (PIC) box and carbonatite worldwide field are from Deines (1989) and Çimen et al. (2018, 2019), respectively. Carbonatites/calcite syenites and marbles (country rock) data of the Karaçayır Complex taken from Cooper et al. (2011). Carbonatite data from the Eskişehir-Kızılcaören Complex and sedimentary limestone data from the Malatya-Kuluncak Complex taken from Çimen et al. (2020).

It is well established that mantle-derived carbonatite melts are enriched in Sr, Nd, REEs, and volatiles (e.g., Bell and Simonetti, 2010; Jones et al., 2013) compared to sedimentary carbonates (<200 ppm for REEs; e.g., Xu et al., 2010). The Karaçayır carbonatites investigated here contain elevated concentrations of Ba, Th, Sr, and REEs, and their trace element PM-normalized and CN REE patterns overlap with those for carbonatites worldwide (Fig. 5; e.g., Çimen et al., 2018, 2019); these features are all clearly indicative of a magmatic origin. Of note, the CN patterns for samples with higher REE concentrations (SVK-1, −2, −8, −11, −12) overlap with those previously reported data by Cooper et al. (2011), and the remaining samples nonetheless also exhibit CN patterns characteristic of carbonatites despite their lower REE concentrations (Fig. 5. The different enrichments levels in CN-REE patterns shown in Fig. 5b may be attributed to the presence of micron-sized inclusions of REE-bearing phases (e.g., apatite, monazite, allanite) in several of the carbonate separates (SVK-1, −2, −8, −11, −12). The main reason being that there is no evidence for the occurrence of a late-stage REE hydrothermal event in the region. Another possible explanation may be related to crustal contamination by the country rock (marble), which may have diluted the total REE contents for the remaining samples (SVK-4, −5, −6, −7, −9, −10). In addition, the B contents of the carbonatites investigated here (Table 1 are distinctly lower than those for bulk continental crust and carbonate sediments (<~10 ppm; Ishikawa and Nakamura, 1993; Marschall et al., 2017), and more akin with those for carbonatites worldwide (<~1 ppm Hulett et al., 2016; Çimen et al., 2018, 2019, 2020; Kuebler et al., 2020, in press). Hence, based on the combined trace elements results reported here, the carbonate separates from the Karaçayır carbonatites are consistent with those for mantle-derived carbonatites rather than sedimentary limestone.

In relation to carbonatite petrogenesis, stable O and C isotope compositions have proven effective in deciphering their origin and the possible effects of post-magmatic/sub-solidus alteration processes (e.g., Keller and Hoefs, 1995; Simonetti et al., 1995). In addition, stable B isotopes have recently been adopted as a valuable forensic tool for deciphering the nature of upper mantle sources for carbonatites (e.g., Hulett et al., 2016; Çimen et al., 2018, 2019, 2020; Kuebler et al., 2020, in press). All carbonate fractions for samples investigated here contain C and O isotope values that plot outside and to the right of the field defined for PIC (Fig. 7, which may be attributed to post-magmatic processes such as low-temperature, sub-solidus alteration (e.g., Deines, 1989; Simonetti et al., 1995). With the exception of samples SVK-4 and −9, the

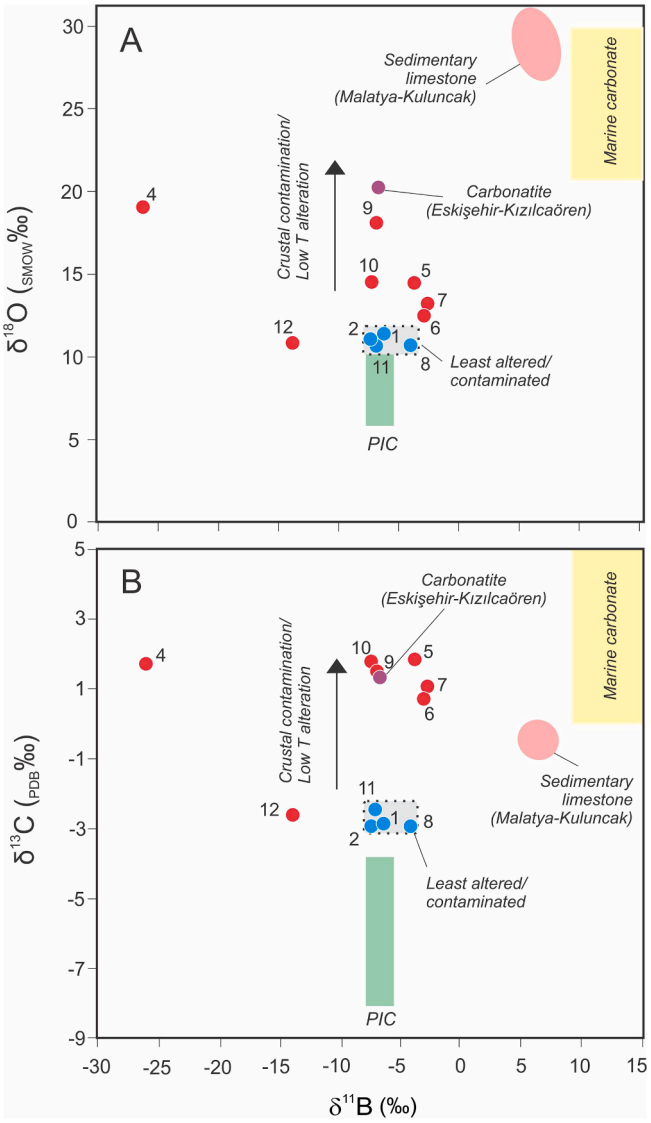

Fig. 8. Diagrams of **A.** $\delta^{18}O$ and **B.** $\delta^{13}C$ compositions vs $\delta^{11}B$ values for carbonate separates from the Karaçayır carbonatite samples. $\delta^{13}C$ and $\delta^{18}O$ values for PIC are from Deines (1989), and asthenospheric $\delta^{11}B$ value for PIC is from Marschall et al. (2017). Marine carbonates data taken from Xue et al. (2018) and Xiao et al. (2013). Carbonatite data from the Eskişehir-Kızılcaören Complex and sedimentary limestone data from the Malatya-Kuluncak Complex taken from Çimen et al. (2020). The blue circles represent the least contaminated/altered carbonatite samples investigated here.

remaining samples plot within the field defined by carbonatite occurrences worldwide, which may still be consistent with a magmatic origin (Fig. 7. However, four samples (SVK-1, −2, −8, −11) are characterized by lighter O (+10.69 to +11.44‰) and C (−2.93 to −2.47‰) isotope compositions and contain the highest concentrations of REEs compared to the remaining carbonatite samples from Karaçayır (Fig. 5. Hence, these four samples may indeed represent either the least altered or contaminated samples of those investigated here, and should therefore be used for evaluating mantle source region characteristics. These four samples record a range of B isotope (−7.4 to −4.2‰) signatures that partly overlap that for asthenospheric mantle (~-7.1 ± 0.9 ‰; Marschall et al., 2017), and therefore corroborate their non-contaminated nature. In contrast, the remaining samples investigated here are characterized by much heavier C and O isotope compositions, associated with less abundant REE contents, and record highly variable B isotope compositions (−25.9 to −2.9‰; Table 2.

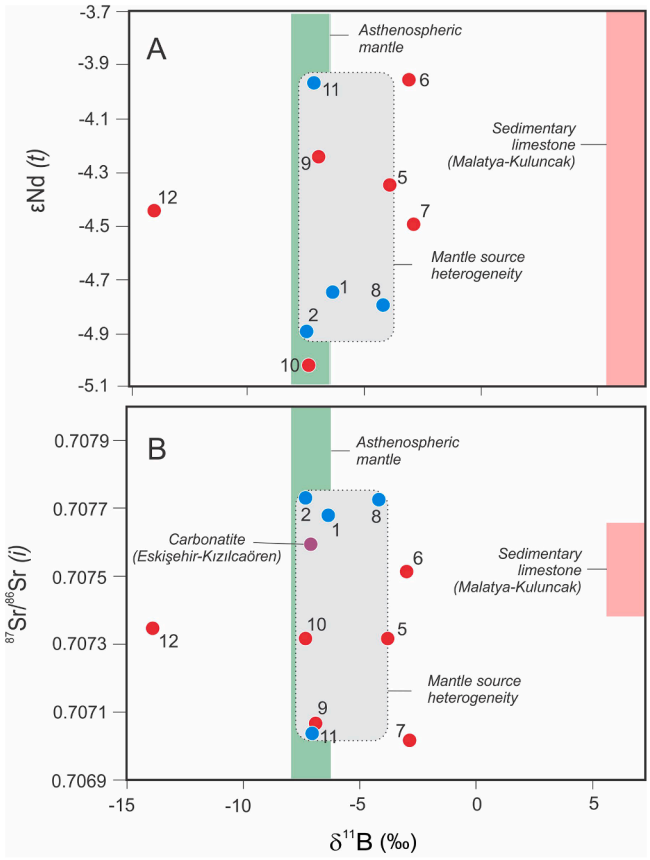

Fig. 9. Diagrams of **A.** $\varepsilon Nd_{(t)}$ and **B.** $^{87}Sr/^{86}Sr_{(i)}$ compositions vs $\delta^{11}B$ values for carbonate separates from the Karaçayır carbonatite samples. Asthenospheric $\delta^{11}B$ value for PIC is from Marschall et al. (2017). Carbonatite data from the Eskişehir-Kızılcaören Complex and sedimentary limestone data from the Malatya-Kuluncak Complex taken from Çimen et al. (2020). The blue circles represent the least contaminated/altered carbonatite samples investigated here. The SVK-4 sample was excluded in this figure due to its extremely depleted $\delta^{11}B$ value.

5.2. *Open system behavior and mantle source characteristics*

With regards to the origin of the Karaçayır carbonatites, two hypotheses have been proposed in previous studies: 1- the carbonatites are the result of assimilation of the host marble into the syenite magma during the emplacement of the latter (Schuiling, 1961), or 2- product of fractional crystallization of a syenitic parental magma (Cooper et al., 2011). The first hypothesis assumes a non-mantle origin for the carbonatite, whereas the latter advocates their derivation by melt differentiation (fractional crystallization) within a closed magma system. On the basis of the combined O, C and B isotope results discussed above (Fig. 8, those for carbonatite samples SVK-1, −2, −8, and −11 from Karaçayır are consistent with a magmatic origin and thus corroborate the second hypothesis (Cooper et al., 2011) cited above. Thus, these four samples represent the most pristine/least altered carbonatite and should be used to evaluate the mantle source region characteristics. Of importance, the evidence for crustal contamination recorded by several of the samples investigated here is not consistent with the closed-system fractional crystallization petrogenetic model proposed by Cooper et al. (2011). This finding is also corroborated by the incompatible trace element systematics of calcite crystals from syenite, calcite-syenite and carbonatite samples, and nonidentical radiogenic isotopes of these rock assemblages. For instance, Ba, Sr and TREE trace elements can be used to monitor fractional crystallization of calcite within carbonatitic melts since they are abundant with magmatic carbonate (Çimen et al., 2018). Here, the comparison of Ba, Sr and TREE contents of calcites are

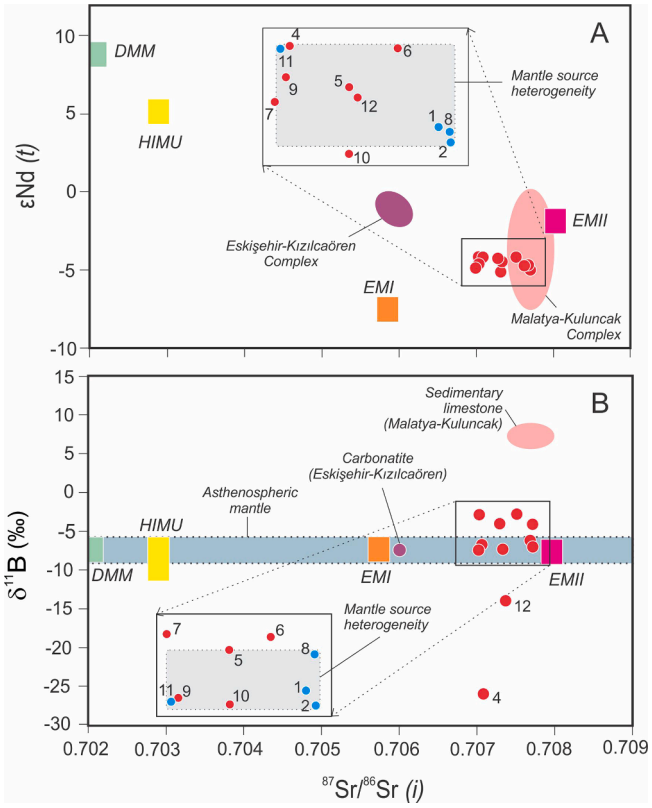

Fig. 10. Diagrams of **A.** $\varepsilon Nd_{(t)}$ and **B.** $\delta^{11}B$ compositions vs $^{87}Sr/^{86}Sr_{(i)}$ values for carbonate separates from the Karaçayır carbonatite samples. HIMU, EMI, EMII and DMM fields are from Zindler and Hart (1986). Asthenospheric $\delta^{11}B$ value (light blue field) is from Marschall et al. (2017) and Walowski et al. (2021). Data from the Eskişehir-Kızılcaören and the Malatya-Kuluncak Complexes taken from Çimen et al. (2020). The blue circles represent the least contaminated/altered carbonatite samples investigated here.

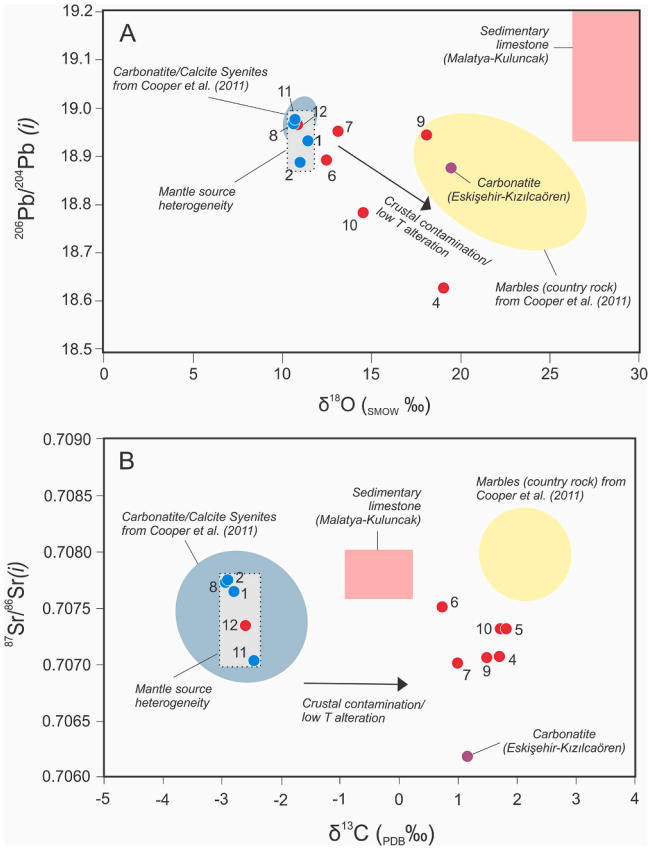

Fig. 11. Diagrams of **A.** $^{206}Pb/^{204}Pb_{(i)}$ and **B.** $^{87}Sr/^{86}Sr_{(i)}$ compositions vs $\delta^{13}C$ values for carbonate separates from the Karaçayır carbonatite samples. Carbonatites/calcite syenites and marbles (country rock) data taken from Cooper et al. (2011). Carbonatite data from the Eskişehir-Kızılcaören Complex and sedimentary limestone data from the Malatya-Kuluncak Complex taken from Çimen et al. (2020). The blue circles represent the least contaminated/altered carbonatite samples investigated here.

completely scattered and do not exhibit any significant correlations (Fig. 6, which rule out the presence of calcite fractionation within a closed system from the syenites to the carbonatites. Moreover, most of the calcite syenites are characterized by higher incompatible Sr and TREE concentrations than the majority of the carbonatites, and these distributions are not considered with a fractional crystallization system from calcite syenites to carbonatites. In addition, the non-identical Sr isotope ratios of carbonatites (0.70702 to 0.70773, Table 3 and syenites (0.70656 to 0.70751; Cooper et al., 2011) support that the carbonatites cannot be derived from the syenites via melt differentiation involving closed system fractional crystallization of a single parental melt. All these evidences suggest that the carbonatites investigated here could have been generated under an open system magmatic evolution including magma mixing and/or crustal contamination/assimilation processes.

$^{87}Sr/^{86}Sr_{(i)}$ and $^{143}Nd/^{144}Nd_{(i)}$ ratios for samples SVK-1, −2, −8, and −11 vary between 0.70704 and 0.70773 and 0.51228 to 0.51231, respectively, which indicate that the Karaçayır carbonatites have been derived from a heterogeneous upper mantle source (Fig. 9. Samples SVK-1, −2, and −8 are characterized by more radiogenic Sr isotope values, whereas sample SVK-11 exhibits a more radiogenic Nd isotopic signature (Figs. 9 and 10. Moreoever, the B isotope ratios (−7.4 to −6.4‰) for samples SVK-1, −2, and −11 overlap those for asthenospheric mantle (~-7.1 ± 0.9 ‰; Marschall et al., 2017), whereas the slightly heavier B isotope value (−4.2‰) for sample SVK-8 may indicate the involment of recycled crustal carbon within its mantle source (Figs. 8, 9 and Table 2. Recent investigations that report combined B, Ca and Sr isotope compositions for carbonatites worldwide are consistent with the presence of recycled crustal carbon in their upper mantle source region, in particular for complexes that are < 300 million years old (e.g., Hulett et al., 2016; Çimen et al., 2018, 2019, 2020; Kuebler et al., 2020, in press; Banerjee et al., 2021). The combined Sr, Nd, and B isotopic systematics for the four least altered/contaminated samples (SVK-1, −2, −8, and −11) suggest that the Karaçayır carbonatites may have been generated from a heterogeneous mantle source characterized by an EM- (enriched mantle; Zindler and Hart, 1986) like signature and contains traces of recycled crustal carbon (Fig. 10.

The Pb isotope compositions for the carbonatite samples from Karaçayir investigated here support the hypothesis that a significant number may have been contaminated by the surrounding country rocks (marble), or have undergone low temperature alteration (Figs. 11 and 12. In particular, the combined $^{206}Pb/^{204}Pb_{(i)}$ vs $\delta^{18}O_{SMOW}$ (‰) diagram (Fig. 11a clearly shows that the isotope signatures for samples SVK-1, −2, −8, and −11 are tightly constrained and plot furthest away from the fields representing the compositions of the host marbles within the region (Fig. 12. Similar to the Sr and Nd isotope signatures discussed above, the Pb isotope values for the least altered or contaminated samples (SVK-1, −2, −8, and −11) may indeed represent those inherited from their mantle source region, which is isotopically heterogeneous and characterized by an EM-like composition (Fig. 12. It should be noted that sample SVK-5 is characterized by an extremely radiogenic $^{206}Pb/^{204}Pb_{(i)}$ value (30.06) relative to the remaining samples, and this may support the involvement of a distinct radiogenic Pb reservoir for carbonatite melt generation; similar radiogenic Pb isotope compositions have been previously reported for carbonatite occurrences worldwide

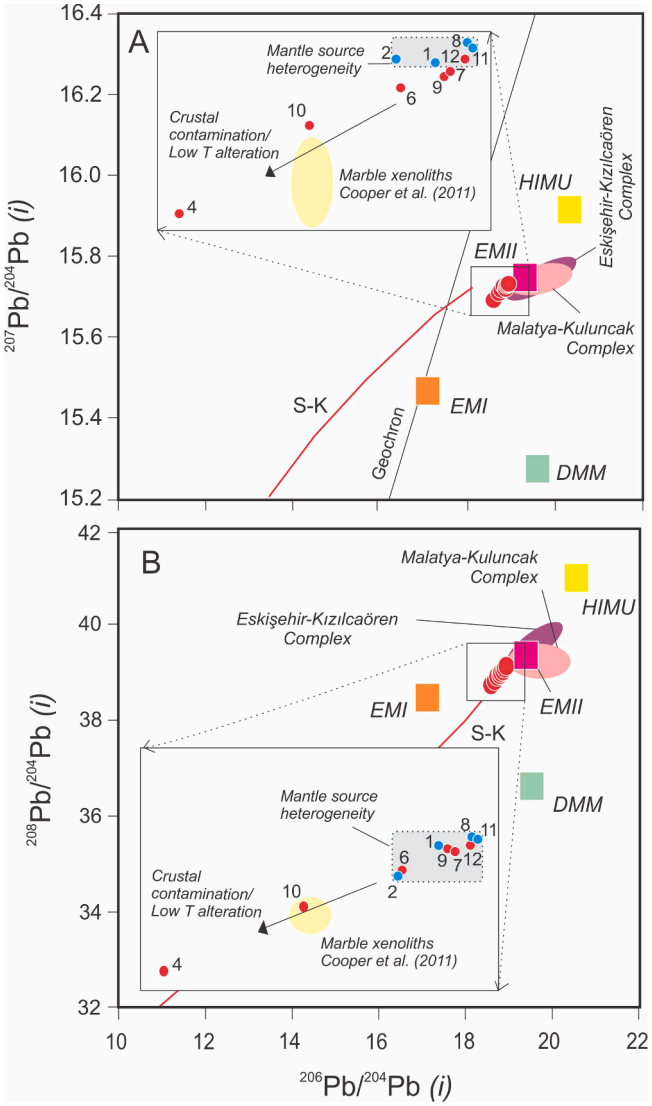

Fig. 12. Diagrams of **A.** $^{207}Pb/^{204}Pb_{(i)}$ and **B.** $^{208}Pb/^{204}Pb_{(i)}$ compositions vs $^{206}Pb/^{204}Pb_{(i)}$ values for carbonate separates from the Karaçayır carbonatite samples. HIMU, EMI, EMII and DMM fields are from Zindler and Hart (1986). Marble xeneliths data taken from Cooper et al. (2011). The 4.56 Ga Geochron is also plotted in A. S-K: Stacey-Kramers 2-stage Pb evolution curve (Stacey and Kramers, 1975). Result for SVK-5 sample was excluded due to extremely radiogenic $^{206}Pb/^{204}Pb_{(i)}$ (30.6) isotope composition. Data from the Eskişehir-Kızılcaören and the Malatya-Kuluncak Complexes taken from Çimen et al. (2020). The blue circles represent the least contaminated/altered carbonatite samples investigated here.

(Andersen, 1987; Chen et al., 2018; Çimen et al., 2018, 2019). One possible explanation is that the mantle source region for the Karaçayir carbonatite contains U-Th accessory minerals found within localized regions of the metasomatized (metasomes) sections of the upper mantle (e.g., Meen et al., 1989). However, this interpretation remains to be thoroughly investigated and is beyond the scope of this study.

Cooper et al. (2011) report similar stable $\delta^{18}O$ (11.31 to 16.49 ‰), $\delta^{13}C$ (−2.11 to −0.94 ‰) and radiogenic $Sr_{(i)}$ (0.70656–0.70751), $^{206}Pb/^{204}Pb_{(i)}$, (18.96 to 19.41), $^{207}Pb/^{204}Pb_{(i)}$ (15.71 to 15.74), $^{208}Pb/^{204}Pb_{(i)}$ (39.11 to 39.89) isotopic data for syenites from the Karaçayır Complex compared to those for the carbonatites from this study. This coincidence in isotopic signatures indicates that the carbonatites and syenites were most likely derived from a common heterogeneous mantle source. However, their non-identical radiogenic isotope ratios and distinct incompatible trace element systematics (Fig. 6 discussed above cannot be reconciled with a closed magmatic system (i.e., fractional crystallization or liquid immiscibility), and suggest that they could have been generated by discrete partial melt fractions from a heterogeneous mantle source, which are not co-genetically related to one parental magma. In summary, the combined stable and radiogenic isotope systematics (Figs. 8 to 12 suggest that the Karaçayır carbonatites were most likely derived from an isotopically heterogeneous mantle source containing EM-like components, which also contained the presence of recycled crustal carbon. The latter interpretation is consistent with the isotope signatures from young (<300 Ma old) carbonatite complexes worldwide (e.g., Hulett et al., 2016; Çimen et al., 2019; Kuebler et al., 2020; Banerjee et al., 2021). Hulett et al. (2016) proposed that upper mantle sources giving rise to carbonatite melts worldwide during the last 300 million years have been significantly impacted by large-scale subduction events associated with supercontinent tectonic cycles.

5.3. Regional geodynamic context

It is well-known that the late Cretaceous-early Paleocene magmatism in the CACC occurred within a post-collisional tectonic setting as a result of closure of the northern Neo-Tethyan Ocean, between the Sakarya Zone in the north and the Anatolide-Tauride Platform in the south (Fig. 1; e.g., Aydın et al., 1998; İlbeyli et al., 2004, Köksal et al., 2004; Boztuğ et al., 2007, 2009). The collision first formed between the central Anatolian ophiolites (representing the island arc of the northern Neo-tethyan ocean) and the Anatolide-Tauride Platform during the Cenomanian–Turonian to the Campanian; whereas the initial continent–continent collision between the Sakarya Zone and the Anatolide-Tauride Platform occured during the Campanian-Maastrichtian (e.g., İlbeyli et al., 2004; Boztuğ et al., 2009). This collision-related crustal thickening and metamorphism was followed by the post-collisional extension regime, and the late Cretaceous-early Paleocene magmatism took place within such a tectonic setting during this time period (e.g., Boztuğ et al., 2007, 2009). İlbeyli et al. (2004, 2009) suggested that initiation of post-collisional magmatism in the CACC may be explained by delamination of the thickened thermal boundary layer, or removal of a subducted plate (slab breakoff) due to the lack of evidence for localized extension. It should be noted that there is substantial consensus in the literature since a similar mechanism has been proposed by several researchers (e.g., Aydın et al., 1998; Boztuğ, 1998, 2000; Köksal et al., 2001; Boztuğ et al., 2007, 2009). The Karaçayır carbonatite complex is located in northeastern region of the CACC, and is composed of monzonite, syenite, granite and carbonatite, and intrudes the Akdağ Metamorphics (Figs. 1 and 2; Schuiling, 1961; Cooper et al., 2011). The syenite of the Karaçayır carbonatite complex has been dated as late Cretaceous (zircon evaporation U-Pb = 99.0 ± 11.0 Ma, Boztuğ et al., 2007; zircon U-Pb = 67.8 ± 1.1 Ma, Cooper et al., 2011), and Paleocene cooling ages (biotite Ar-Ar = 65–66 Ma; Boztuğ et al., 2009) have been reported for the same rock type. In this study, for the first time, a late Cretaceous age of 69.3 ± 1.7 Ma is reported for apatite from carbonatite (Fig. 12, which is consistent with the age for the calcite syenite reported by Cooper et al. (2011); this result indicates that syenite and carbonatite magma emplacement was most likely coeval.

Of importance, the Karaçayır carbonatite complex represents one of the significant rare earth element (REE) mineralizations in Turkey, in addition to those of the Eskişehir-Kızılcaören and Malatya-Kuluncak occurrences (Fig. 1; e.g., Özgenç, 1993; Öztürk et al., 2019a,b; Çimen et al., 2020). In the CACC, the Malatya-Kuluncak Complex may have formed in a post-collisional tectonic setting during the late Cretaceous-early Paleocene period following the collision of the Tauride-Anatolide Platform with the Central Anatolian Ophiolite and the Eastern Pontides, respectively (Fig. 1; Boztuğ et al., 2009; Özgenç and İlbeyli, 2009; Çimen et al., 2020). The Sivas-Karaçayır Complex may have been derived within a similar tectonic setting as that for the Malatya-Kuluncak Complex, and the presence of an enriched upper mantle source has

Table 5
In-situ U-Pb dating results for apatites by LA-MC-ICP-MS.

Sample/ Anal.	^{206}Pb cps	^{238}U cps	^{238}U/^{206}Pb	2 s error	^{207}Pb/^{206}Pb	2 s error	Rad. Frac. ^{206}Pb	^{206}Pb/^{238}U Rad.	^{206}Pb/^{238}U Rad. Age (Ma)	2 s error
SVK-1 / 1	114,616	4,301,657	30.576	2.141	0.5892	0.0118	0.32	0.0104	66.4	4.7
SVK-1 / 2	107,247	3,981,115	30.289	2.121	0.5880	0.0118	0.32	0.0105	67.4	4.7
SVK-1 / 3	112,988	5,288,392	38.133	2.672	0.5387	0.0108	0.38	0.0100	64.0	4.5
SVK-1 / 4	103,962	3,623,394	28.458	1.993	0.5946	0.0119	0.31	0.0109	69.8	4.9
SVK-1 / 5	96,804	3,530,854	29.756	2.083	0.5863	0.0118	0.32	0.0108	69.0	4.8
SVK-1 / 6	85,803	2,481,774	23.581	1.665	0.6259	0.0127	0.27	0.0115	73.5	5.2
SVK-2 / 1	62,424	2,187,684	28.666	2.007	0.5917	0.0119	0.31	0.0109	70.1	4.9
SVK-2 / 2	72,503	2,498,047	28.126	1.969	0.5909	0.0118	0.31	0.0112	71.7	5.0
SVK-2 / 3	82,428	2,750,102	27.269	1.910	0.5938	0.0119	0.31	0.0114	73.1	5.1
SVK-2 / 4	83,221	2,776,856	27.315	1.914	0.5950	0.0120	0.31	0.0113	72.6	5.1
SVK-2 / 5	66,173	1,567,182	26.850	1.881	0.5946	0.0119	0.31	0.0115	74.0	5.2
SVK-8 / 1	11,723	1,063,070	72.040	5.048	0.1914	0.0041	0.82	0.0114	72.8	5.1
SVK-8 / 2	16,616	1,502,189	74.924	5.365	0.2482	0.0141	0.75	0.0100	63.9	4.6
SVK-8 / 3	104,050	12,373,509	95.752	6.724	0.0894	0.0023	0.95	0.0099	63.4	4.5
SVK-8 / 6	12,985	1,166,287	71.669	5.026	0.2208	0.0053	0.78	0.0109	69.9	4.9
SVK-12 / 1	99,184	2,226,016	21.203	1.500	0.6478	0.0130	0.24	0.0114	73.4	5.2
SVK-12 / 2	98,576	2,906,575	27.330	1.913	0.6103	0.0122	0.29	0.0106	68.0	4.8
SVK-12 / 3	25,828	716,733	25.717	1.806	0.6191	0.0125	0.28	0.0108	69.5	4.9
SVK-12 / 4	52,128	1,237,881	22.064	1.546	0.6351	0.0128	0.26	0.0117	75.1	5.3
SVK-12 / 5	53,343	1,249,247	21.703	1.544	0.6626	0.0134	0.22	0.0103	66.2	4.7

Rad. = Radiogenic; Frac. = Fraction.

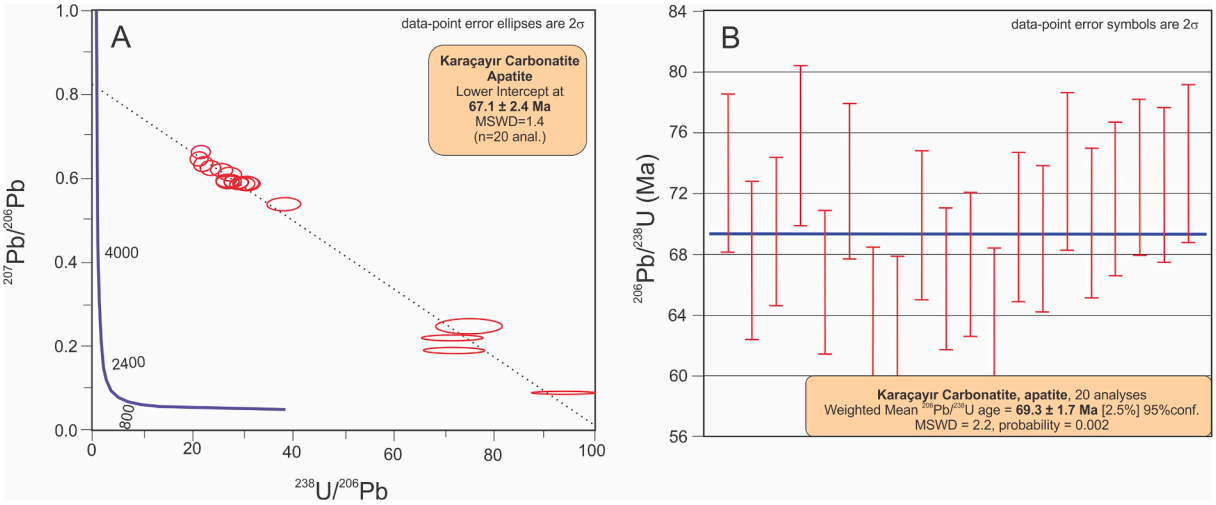

Fig. 13. A. ^{207}Pb/^{206}Pb vs ^{238}U/^{206}Pb and **B.** ^{206}Pb/^{238}U diagrams illustrating lower intercept and weighted mean ages for apatite crystals from the Karaçayır carbonatite samples, respectively (SVK-1, 2, 8, 12; n = 20 analyses).

also been suggested for derivation of late Cretaceous-early Paleocene A-type granitoids from the Hamit, Çamsarı, Divriği, Hasançelebi and Keban regions in the CACC (Fig. 1; e.g., İlbeyli et al., 2004; Boztuğ et al., 2007; Köksal and Göncüoğlu, 2008; Kuşcu et al., 2011; Kürüm, 2013; Çimen et al., 2020). The available $Sr_{(i)}$ (0.70424–0.71071), $Nd_{(i)}$ (0.51218–0.51260), $^{206}Pb/^{204}Pb_{(i)}$, (18.57 to 18.96), $^{207}Pb/^{204}Pb_{(i)}$ (15.64 to 15.69) and $^{208}Pb/^{204}Pb_{(i)}$ (38.69 to 38.80) isotope data reported from these regions are consistent with those from the Karaçayır carbonatites (Tables 3 and 4, and indicate the presence of an isotopically heterogeneous, enriched mantle source beneath the eastern-central Anatolide-Tauride Platform during the late Cretaceous.

In contrast, in western Turkey (Fig, 1), the Eskişehir-Kızılcaören Complex is located within the Sakarya Zone to the north of İzmir-Ankara-Erzincan Suture Belt (remnant of the northern branch of Neotethyan ocean). This complex is characterized by lower $Sr_{(i)}$ (0.70584–0.70636) and higher $Nd_{(i)}$ (0.51256–0.51258) isotope compositions (Çimen et al., 2020) compared to Sr and Nd isotope compositions for magmatic complexes from the CACC cited above, which indicates derivation from a distinct mantle source region. It is well-established that the period of alkaline magmatism in western Anatolia is associated with widespread I-type volcanism within a *syn*-convergent extensional setting during the late Oligocene to middle Miocene (Altunkaynak et al., 2012; Ersoy et al., 2012; Gencer et al., 2020). These magmatic rocks are characterized by variable $Sr_{(i)}$ (0.70450–0.70868), $Nd_{(i)}$ (0.51231–0.51275), $^{206}Pb/^{204}Pb_{(i)}$, (18.75 to 19.11), $^{207}Pb/^{204}Pb_{(i)}$ (15.71 to 15.76) and $^{208}Pb/^{204}Pb_{(i)}$ (38.96 to 39.34) values (e.g., Aldanmaz et al., 2000; Temel, 2001; Sarıfakıoğlu et al., 2009), and these compositions are consistent with those from the Eskişehir-Kızılcaören Complex (Çimen et al., 2020), which indicate the presence of a heterogeneous, enriched mantle source for alkaline magmatism in the region. Therefore, the Eskişehir-Kızılcaören Complex may have been derived from an enriched/metasomatized lithospheric mantle source within an extensional tectonic setting in the Sakarya Zone during the late Oligocene-early Miocene time (Fig. 1.; Sarıfakıoğlu et al., 2009; Nikiforov et al., 2014; Çimen et al., 2020).

Overall, comparison between the isotope data for the REE occurrences at Karaçayır and Malatya-Kuluncak located in the eastern Anatolide-Tauride Platfrom and those for Eskişehir-Kızılcaören indicate that the former two were derived from a more enriched, metasomatized mantle source, which most likely involved subduction-related

components in a post-collisional tectonic setting during the late Cretaceous-early Paleocene. In contrast, the latter formed in an extensional setting within the Sakarya Zone during the late Oligocene-early Miocene (Fig. 1.

6. Conclusions

The combined stable (B, O and C) and radiogenic isotope (Sr, Nd, Pb), and in-situ apatite U-Pb dating results from the Karaçayır carbonatite reported here provide more detailed information about its petrogenetic evolution, tectonic setting during emplacement, and chemical nature of its mantle source(s); the main interpretations are the following:

- The combined trace element, stable and radiogenic isotope data for carbonate separates clearly indicate their magmatic origin. A significant number of samples may have been either contaminated by surrounding crustal country rocks or underwent low-temperature alteration.
- The geochemical and isotope characteristics of the most pristine/least altered carbonate samples suggest that the carbonatite magma at Karaçayır most likely represents a low-degree partial melt of an isotopically heterogeneous (metasomatized) mantle source containing EM-like components and recycled crustal carbon. This interpretation is consistent with those from young (<300 Ma) carbonatite complexes worldwide.
- Overall, the data presented in this study cannot be reconciled with melt differentiation involving closed system fractional crystallization of a single parental melt.
- In-situ U-Pb results for apatite present within the carbonatites indicate that the Karaçayır complex formed during the late Cretaceous within a post-collisional tectonic setting following the collision of the Anatolide-Tauride Platform with the central Anatolian ophiolite and the Sakarya Zone.
- In relation to the magmatic and tectonic evolution of the main REE complexes in Turkey, the Karaçayır and Malatya-Kuluncak Complexes were derived from a more enriched, heterogeneous mantle source within a similar post-collisional environment compared with the Eskişehir-Kızılcaören Complex; the latter formed in an extensional setting within the Sakarya Zone during the late Oligocene-early Miocene.

Declaration of Competing Interest

The authors declare that they have no known competing financial interests or personal relationships that could have appeared to influence the work reported in this paper.

Acknowledgements

We thank Dr. Dana Biasatti (CEST) for assistance with O and C isotope analyses. This research was financially supported by the General Directorate of Mineral Research and Exploration of Turkey (Project number: 2019-32-13-23) and the University of Notre Dame. We appreciate the comments provided by Dr. Alan F. Cooper and an anonymous reviewer, which have resulted in an improved manuscript. Also, we would like to thank Dr. İbrahim Uysal (Associate Editor) for handling our manuscript.

References

Aldanmaz, E., Pearce, J.A., Thirwall, M.F., Mitchell, J.G., 2000. Petrogenetic evolution of Late Cenozoic post-collision volcanism in western Anatolia. Turkey. J. Volcanol. Geoth. Res. 102, 67–95.

Altunkaynak, S., Dilek, Y., Genc, C.S., Sunal, G., Gertisser, R., Furnes, H., Foland, K.A., Yang, J., 2012. Spatial, temporal and geochemical evolution of Oligo–Miocene granitoid magmatism in western Anatolia, Turkey. Gondwana Res. 21, 961-98.

Andersen, T., 1987. Mantle and crustal components in a carbonatite complex, and the evolution of carbonatite magma: REE and isotopic evidence from the Fen complex, S. E. Norway. Chem. Geol. Isotope Geosci. Sect. 65, 147–166.

Anenburg, M., Mavrogenes, J.A., Bennett, V.C., 2020. The Fluorapatite P-REE–Th Vein Deposit at Nolans Bore: Genesis by Carbonatite Metasomatism. J. Petrol. 61, 1.

Aydın, S.N., Göncüoğlu, M.C., Erler, A., 1998. Latest Cretaceous magmatism in the CACC: Review of field, petrographic and geochemical features. Turkish J. Earth Sci. 7, 259–268.

Banerjee, A., Chakrabarti, R., Simonetti, A., 2021. Temporal evolution of $\delta^{44/40}$Ca and $^{87}Sr/^{86}Sr$ of carbonatites: Implications for crustal recycling through time. Geochim. Cosmochim. Acta 307, 168-191.

Barakos, G., Mischo, H., Gutzmer, J., 2015. Status Quo and Future Evaluations of Global Rare Earth Mining (with Respect to Special Rare Earth Element-industry Criteria). Third International Future Mining Conference / Sydney, NSW 4–6.

Bell, K., Kjarsgaard, B.A., Simonetti, A., 1998. Carbonatites - into the twenty-first century. J. Petrol. 39, 1839–1845.

Bell, K., Simonetti, A., 2010. Source of parental melts to carbonatites–critical isotopic constraints. Mineral. Petrol. 98, 77–89.

Beyazpirinç, M., Akçay, A.E., Özkan, M.K., Sönmez, M.K., Dönmez, M., 2021. The new age data and pre-Tertiary stratigraphy of the Kırşehir Massif. Central Anatolia. Bull. Min. Res. Exp. 1–31.

Boztuğ, D., 1998. Post-collisional central Anatolian alkaline plutonism. Turkey. Turkish J. Earth Sci. 7, 145–165.

Boztuğ, D., 2000. S–I–A-type intrusive associations: geodynamic significance of synchronism between metamorphism and magmatism in Central Anatolia, Turkey. In: Bozkurt, E., Winchester, J., Piper, J.A. (Eds.), Tectonics and Magmatism in Turkey and the Surrounding Area. Geol. Soc. Spec. Publ. 173, 407-424.

Boztuğ, D., Harlavan, Y., Arehart, G.B., Satır, M., Avci, N., 2007. K-Ar age, whole-rock and isotope geochemistry of A-type granitoids in the Divriği-Sivas region, eastern-central Anatolia, Turkey. Lithos 97, 193–218.

Boztuğ, D., Türksever, E., Heizler, M., Jonckheere, R.C., Tichomirowa, M., 2009. 207Pb-206Pb, 40Ar-39Ar and apatite fission-track geothermochronology revealing the emplacement, cooling and exhumation history of the Karacayır Syenite (N Sivas), East Central Anatolia. Turkey. Turkish J. Earth Sci. 18, 109–125.

Chakhmouradian, A.R., Wall, F., 2012. Rare earth elements: minerals, mines, magnets (and more). Elements 8, 333–340.

Chakhmouradian, A.R., Reguir, E.P., Kressall, R.D., Crozier, J., Pisiak, L.K., Sidhu, R., Yang, P., 2015. Carbonatite-hosted niobium deposit at Aley, northern British Columbia (Canada): Mineralogy, geochemistry and petrogenesis. Ore Geol. Rev. 64, 642–666.

Chen, W., Simonetti, A., 2014. Evidence for the multi-stage petrogenetic history of the Oka carbonatite complex (Québec, Canada) as recorded by perovskite and apatite. Minerals 4, 437–476.

Chen, W., Lu, J., Jiang, S.Y., Ying, Y.C., Liu, Y.S., 2018. Radiogenic Pb reservoir contributes to the rare earth element (REE) enrichment in South Qinling carbonatites. Chem. Geol. 494, 80–95.

Çimen, O., Kuebler, C., Monaco, B., Simonetti, S.S., Corcoran, L., Chen, W., Simonetti, A., 2018. Boron, Carbon, Oxygen and Radiogenic Isotope Investigation of Carbonatite from the Miaoya complex, central China: Evidences for late-stage REE hydrothermal event and mantle source heterogeneity. Lithos 322, 225–237.

Çimen, O., Kuebler, C., Simonetti, S.S., Corcoran, L., Mitchell, R., Simonetti, A., 2019. Combined Boron, Radiogenic (Nd, Pb, Sr), Stable (C, O) Isotopic and Geochemical Investigations of Carbonatites From the Blue River Region, British Columbia (Canada): Implications for Mantle Sources and Recycling of Crustal Carbon. Chem. Geol. 529, 119240.

Çimen, O., Corcoran, L., Kuebler, C., Simonetti, S.S., Simonetti, A., 2020. Geochemical, stable (O, C and B) and radiogenic (Sr, Nd, Pb) isotopic data from the Eskişehir-Kızılcaören (NW-Anatolia) and the Malatya-Kuluncak (E-central Anatolia) F-REE-Th deposits, Turkey: Implications for nature of carbonate-hosted mineralization. Turkish J. Earth Sci. 29, 798–814.

Cooper, A.F., Boztuğ, D., Palin, J.M., Martin, C.E., Numata, M., 2011. Petrology and petrogenesis of carbonatitic rocks in syenites from central Anatolia. Turkey. Contrib. to Mineral. Petrol. 161, 811–828.

Deines, P., 1989. Stable Isotope Variations in Carbonatites: Carbonatites: Genesis and Evolution. Unwin Hyman. 13, 301–359.

Delaloye, M., Özgenç, İ., 1983. Petrography and age determinations of the alkaline volcanic rocks and carbonatite of Kızılcaören district, Beylikahır-Eskişehir. Turkey. Swiss Bull. Mineral. Petrol. 63, 289–294.

Dushyantha, N., Batapola, N., Ilankoon, I.M.S.K., Rohitha, S., Premasiri, R., Abeysinghe, B., Ratnayake, N., Dissanayake, K., 2020. The story of rare earth elements (REEs): Occurrences, global distribution, genesis, geology, mineralogy and global production. Ore Geol Rev 122, 103521.

Ersoy, Y.E., Helvacı, C., Uysal, İ., Karaoğlu, Ö., Palmer, M.R., Dindi, F., 2012. Petrogenesis of the Miocene volcanism along the İzmir-Balıkesir Transfer Zone in western Anatolia, Turkey: Implications for origin and evolution of potassic volcanism in post-collisional areas. J. Volcanol. Geoth. Res. 241–242, 21–38.

European Commission, 2020. Critical Raw Materials Resilience: Charting a Path towards greater Security and Sustainability. Report.

Floyd, P.A., Göncüoğlu, M.C., Winchester, J.A., Yalınız, M.K., 2000. Geochemical character and tectonic environment of Neotethyan ophiolitic fragments and metabasites in the Central Anatolian Crystalline Complex, Turkey. In: Bozkurt, E., Winchester, J., Piper, J.D.A. (Eds.), Tectonics and Magmatism in Turkey and the Surrounding Area. Geol. Soc. Spec. Publ. 173, 183-202.

Gencer, S.B., Erkül, S.T., Erkül, F., 2020. Evolution of slab tearing-related high potassium volcanism: Petrogenetic data from the Emirdağ and İscehisar volcanic units. Bull. Min. Res. Exp. 163, 167–185.

Goodenough, K.M., Schilling, J., Jonsson, E., Kalvig, P., Charles, N., Tuduri, J., Deady, E. A., Sadeghi, M., Schiellerup, H., Müller, A., Bertrand, G., Arvanitidis, N., Eliopoulos, D.G., Shaw, R.A., Thrane, K., Keulen, N., 2016. Europe's rare earth element resource potential: an overview of REE metallogenetic provinces and their geodynamic setting. Ore Geol. Rev. 72, 838–856.

Göncüoğlu, M.C., Toprak, V., Kuşcu, İ., Erler, A., Olgun, E., 1991. Geology of the western part of the Central Anatolian Massif, Part 1: Southern Section: Unpubl. Report No.2909, Turkish Petroleum Company Report (in Turkish).

Göncüoğlu, M.C., Kozlu, H., Dirik, K., 1997. Pre-alpine and alpine terranes in Turkey: explanatory notes to the terrane map of Turkey. Ann. Géol. Pays. Hellén. 37, 515–536.

Güleç, N., 1994. Rb–Sr isotope data from the Ağaçören granitoid (east of Tuz Gölü): geochronological and genetical implications. Turkish J. Earth Sci. 3, 39–43.

Gültekin, A.H., Örgün, Y., Suner, F., 2003. Geology, mineralogy and fluid inclusion data of the Kizilcaoren fluorite- barite- REE deposit, Eskisehir. Turkey. J. Asian Earth Sci. 21, 365–376.

Hulett, S.R.W., Simonetti, A., Rasbury, E.T., Hemming, N.G., 2016. Recycling of subducted crustal components into carbonatite melts revealed by boron isotopes. Nat. Geosci. 9, 904–908.

Ishikawa, T., Nakamura, E., 1993. Boron isotope systematics of marine sediments. Earth Planet. Sci. Lett. 117, 567–580.

İlbeyli, N., Pearce, J.A., Thirlwall, M.F., Mitchell, J.G., 2004. Petrogenesis of collision-related plutonics in Central Anatolia, Turkey. Lithos 72, 163–182.

İlbeyli, N., 2005. Mineralogical–geochemical constraints on intrusives in central Anatolia, Turkey: tectono-magmatic evolution and characteristics of mantle source. Geol. Mag. 142, 187–207.

İlbeyli, N., Pearce, J.A., Meighan, I.G., Fallick, A.E., 2009. Contemporaneous Late Cretaceous Calc-alkaline and Alkaline Magmatism in Central Anatolia, Turkey: Oxygen Isotope Constraints on Petrogenesis. Turkish J. Earth. Sci. 18, 529–547.

İnan, N., İnan, S., 1999. New findings on the age and depositional conditions from the Tokus Formation (Sivas, Turkiye). Geol. Bull. Turkey 42, 119–130 (in Turkish with English abstract).

Jones, A.P., Genge, M., Carmody, L., 2013. Carbonate melts and carbonatites. Rev. Mineral. Geochem. 75, 289–322.

Kaplan, H., 1977. Rare earth elements and thorium complex deposit of Kizilcaören village, Sivrihisar-Eskişehir. Turkey. Bull. Geol. Eng. 2, 69–76.

Keller, J., Hoefs, J., 1995. Stable Isotope Characteristics of Recent Natrocarbonatites from Oldoinyo Lengai. Carbonatite Volcanism, IAVCEI Proceedings in Volcanology 4, 113–123.

Koçak, K., Leake, B.E., 1994. The petrology of the Ortaköy district and its ophiolite at the western edge of the Middle Anatolian Massif. Turkey. J. African Earth Sci. 18 (2), 163–174.

Kogarko, L.N., Sorokhtina, N.V., Zaitsev, V.A., Senin, V.G., 2009. Rare Metal Mineralization of Calcite Carbonatites from the Cape Verde Archipelago. Geochemistry Int. 47, 531–549.

Köksal, S., Göncüoğlu, M.C., Floyd, P.A., 2001. Extrusive Members of Postcollisional A-Type Magmatism in Central Anatolia: Karahidir Volcanics, Idis Dagi-Avanos Area, Turkey. Int. Geol. Rev. 43, 683–694.

Köksal, S., Romer, R.L., Göncüoğlu, M.C., Toksoy-Köksal, F., 2004. Timing of post-collision H-type to A-type granitic magmatism: U-Pb titanite ages from the Alpine central Anatolian granitoids Turkey. Int. J. Earth Sci. 93, 974–989.

Köksal, S., Göncüoğlu, M.C., 2008. Sr and Nd Isotopic Characteristics of some S-, I- and A-type Granitoids from Central Anatolia. Turkish J. Earth Sci. 17, 111–127.

Kuebler, C., Simonetti, A., Chen, W., Simonetti, S.S., 2020. Boron isotopic investigation of the Bayan Obo carbonatite complex: Insights into the source of mantle carbon and hydrothermal alteration. Chem. Geol. 557, 119859.

Kuebler, C., Simonetti, A., Simonetti, S.S., Martin, R.F., (in press). Boron isotope compositions establish the origin of marble from metamorphic complexes: Québec, New York, and Sri Lanka. Am. Mineral. https://doi.org/10.2138/am-2021-7811.

Kuşcu, İ., Yılmazer, E., Güleç, N.T., Bayır, S., Demirela, G., Gençalioğlu Kuşcu, G., Sezerer Kuru, G., Kaymakçı, N., 2011. U-Pb and ^{40}Ar-^{39}Ar geochronology and isotopic constraints on the genesis of copper gold bearing iron oxide deposits in the Hasançelebi district eastern Turkey. Econ. Geol. 106, 261–288.

Kuşcu, İ., Tosdal, R.M., Gençalioğlu-Kuşcu, G., Friedman, R., Ullrich, T.D., 2013. Late Cretaceous to Middle Eocene magmatism and metallogeny of a portion of the Southeastern Anatolian Orogenic Belt, east central Turkey. Econ. Geol. 108, 641–666.

Kürüm, S., 2013. Geochemical and Sr Nd isotopic significance of post collisional Keban a type syenites Elazığ Southeastern Turkey. Carpathian J. Earth Environ. Sci. 8 (4), 209–220.

Kynicky, J., Smith, M.P., Xu, C., 2012. Diversity of rare earth deposits: the key example of China. Elements 8, 361–367.

Lefebvre, C.J.C., 2011. The tectonics of the Central Anatolian crystalline complex: a structural, metamorphic and paleomagnetic study. PhD Thesis. Utrecht University, p. 139.

Machacek, E., Kalvig, P., 2016. EURARE European REE market survey. Roadmap for the REE material supply autonomy in Europe. http://www.eurare.org/publications.html.

Marschall, H.R., Wanles, V.D., Shimizu, N., Pogge Von Strandmann, P.A.E., Elliott, T., Monteleone, B.D., 2017. The boron and lithium isotopic composition of mid-ocean ridge basalts and the mantle. Geochim. Cosmochim. Acta 207, 102–138.

Meen, J.K., Ayers, J.C., Fregeau, E.J., 1989. A model of mantle metasomatism by carbonate alkaline melts: trace-element and isotopic compositons of mantle source regions of carbonatite and other continental igneous rocks. In: Bell, K. (Ed.), Carbonatites: genesis and evolution. Unwin Hyman, London, pp. 464–499.

Mitchell, R.H., 2005. Carbonatites and carbonatites and carbonatites. Can. Mineral. 43, 2049–2068.

MTA, 2002. 1:500,000 Geological Map of Turkey. Maden Tektik ve Arama Enstitüsü (MTA), Ankara, Turkey.

Nikiforov, A.V., Öztürk, H., Altuncu, S., Lebedev, V.A., 2014. Kizilcaören Ore-bearing Complex with Carbonatites (Northwestern Anatolia, Turkey): Formation Time and Mineralogy of Rocks. Geol. Ore Depos. 56, 35–60.

Özgenç, İ., 1993. Geology and REE-geochemistry of carbothermal bastnaesite–fluorite–barite deposit of Kızılcaören (Sivrihisar, Eskişehir). Geol. Bull. Turkey 36, 1–11.

Özgenç, İ., Kibici, Y., 1994. The geology and chemical-mineralogical properties of Britholite veins of Başören village (Kuluncak-Malatya). Geol. Bull. Turkey 37, 77–85.

Özgenç, İ., İlbeyli, N., 2009. Geochemical constraints on petrogenesis of Late Cretaceous alkaline magmatism in east-central Anatolia (Hasancelebi–Basören, Malatya). Turkey. Mineral. Petrol. 95, 71–85.

Özkan, M., Çelik, Ö.F., Marzoli, A., Çörtük, R.M., Billor, M.Z., 2021. The origin of carbonatites from the eastern Armutlu Peninsula (NW Turkey). J. Geol. Soc. London. https://doi.org/10.1144/jgs2020-171.

Öztürk, H., Altuncu, S., Hanilçi, N., Kasapçı, C., Goodenough, K.M., 2019a. Rare earth element-bearing fluorite deposits of Turkey: An overview. Ore Geol. Rev. 105, 423–444.

Öztürk, H., Hanilçi, N., Altuncu, S., Kasapçı, C., 2019b. Rare earth element (REE) resources of Turkey: An overview of their characteristics and origin. Bull. Min. Res. Exp. 159, 129–143.

Rosatelli, G., Stoppa, F., Jones, A.P., 2000. Intrusive calcio-carbonatite occurrences from Mt. Vulture volcano, southern Italy. Mineral. Mag. 64, 615–624.

Sarıfakıoğlu, E., Öze,n H., Hall, C., 2009. Petrogenesis of extension-related alkaline volcanism in Karaburhan (Sivrihisar–Eskisehir), NW Anatolia, Turkey. J. Asian Earth Sci. 35, 502-515.

Schuiling, R.D., 1961. Formation of pegmatitic carbonatite in a syenite-marble contact. Nature 192, 1280.

Simonetti, A., Bell, K., Viladkar, S.G., 1995. Isotopic data from the Amba Dongar Carbonatite Complex, west-central India: Evidence for an enriched mantle source. Chem. Geol. 122, 185–198.

Spivack, A.J., Edmond, J.M., 1987. Boron isotope exchange between seawater and the oceanic crust. Geochim. Cosmochim. Acta 51, 1033–1043.

Stacey, J.S., Kramers, J.D., 1975. Approximation of terrestrial lead isotope evolution by a two-stage model. Earth Planet. Sci. Lett. 26, 207–221.

Statista, 2020. Major countries in rare earth mine production worldwide in 2018 and 2019. www.statista.com.

Sun, S.S., McDonough, W.F., 1989. Chemical and isotopic systematics of oceanic basalts: implications for mantle composition and processes. Geol. Soc. London Spec. Publ. 42, 313–345.

Şengör, A.M.C., Yılmaz, Y., 1981. Tethyan evolution of Turkey: a plate tectonic approach. Tectonophysics 75, 181–241.

Temel, A., 2001. Post-collision Miocene alkaline volcanism in the Oglakçi Region, Turkey: petrology and geochemistry. Int. Geol. Rev. 43, 640–660.

United States Geological Survey, 2020. Rare Earths. Mineral Commodity Summaries. 132.

Vrublevskii, V.V., Bukharova, O.V., Nebera, T.S., Sveshnikova, V.L., 2019. Composition and origin of rare-metal (Nb–Ta, REE) and sulfide mineralization in magnesiocarbonatites from the Yenisei Ridge, Central Siberia. Ore Geol. Rev. 111, 102949.

Walowski, K.J., Kirstein, L.A., De Hoog, J.C.M., Elliott, T., Savov, I.P., Jones, R.E., E.I.M. F., 2021. Boron recycling in the mantle: Evidence from a global comparison of ocean island basalts. Geochim. Cosmochim. Acta 302, 83-100.

Walters, A., Lusty, P., Hill, A., 2011. Rare earth elements: mineral profile series [online], British Geological Survey, commodity profilesWhitney, D.L., Teyssier, C., Dilek, Y., Fayon, A.K., 2001. Metamorphism of the Central Anatolian Crystalline Complex, Turkey: influence of orogen-normal collision vs. wrench dominated tectonics on P-T-t paths. J. Metamorph. Geol. 19, 411–432.

Whitney, D.L., Teyssier, C., Fayon, A.K., Hamilton, M.A., Heizler, M., 2003. Tectonic controls on metamorphism, partial melting, and intrusion: timing and duration of regional metamorphism and magmatism in the Nigde Massif, Turkey. Tectonophysics 376, 37–60.

Whitney, D.L., Hamilton, M.A., 2004. Timing of high-grade metamorphism in central Turkey and the assembly of Anatolia. J. Geol. Soc. London 161, 823–828.

Woolley, A.R., 1989. The Spatial and Temporal Distribution of Carbonatites: Carbonatites: Genesis and Evolution. Unwin Hyman 15–37.

Woolley, A.R., Church, A.A., 2005. Extrusive carbonatites: a brief review. Lithos 85, 1–14.

Woolley, A.R., Kjarsgaard, B.A., 2008. Carbonatite occurrences of the world: Map and database. Geological Survey of Canada, Open File Rep, p. 5796.

Wunder, B., Meixner, A., Romer, R.L., Wirth, R., Heinrich, W., 2005. The geochemical cycle of boron: constraints from boron isotope partitioning experiments between mica and fluid. Lithos 84, 206–216.

Xiao, J., Xiao, Y.K., Jin, Z.D., He, M.Y., Liu, C.Q., 2013. Boron isotope variations and its geochemical application in nature. Aust. J. Earth Sci. 60 (4), 431–447.

Xu, C., Wang, L., Song, W., Wu, M., 2010. Carbonatites in China: A review for genesis and mineralization. Geosci. Front. 1, 105–114.

Xue, S., Ling, M.X., Liu, Y.L., Sun, W., 2018. Recycling of subducted carbonates: Formation of the Taohuala Mountain carbonatite, North China Craton. Chem. Geol. 478, 89–101.

Yaliniz, M.K., Floyd, P.A., Göncüoğlu, M.C., 2000. Geochemistry of volcanic rocks from the Cicekdag ophiolite, Central Anatolia, Turkey and their inferred tectonic setting within the northern branch of the NeoTethyan Ocean. In: Bozkurt, E., Winchester, J.

A., Piper, J.D.A. (Eds.), Tectonics and Magmatism in Turkey and the Surrounding Areas, 173. Publ, Geol. Soc. Spec, pp. 203–218.
Zhou, B., Li, Z., Chen, C., 2017. Global Potential of Rare Earth Resources and Rare Earth Demand from Clean Technologies. Minerals 7, 203.
Zindler, A., Hart, S.R., 1986. Chemical dynamics. Annu. Rev. Earth Planet. Sci. 14, 493–571.